Journal of Applied Mechanics and Technical Physics, Vol. 36, No. 4, 1995

FORMATION AND DEVELOPMENT OF COHERENT STRUCTURES IN A TRANSITIONAL BOUNDARY LAYER

V. I. Borodulin and Y. S. Kachanov

UDC 532.526

1. **Introduction.** It is known that two main ways of breakdown of the laminar regime in a boundary layer are observed when the level of external disturbances is not too high. These are the K-regime, discovered over thirty years ago in experiments [1–3], and the N-regime (or the subharmonic one), found in experiments [4]. A brief review of the earlier studies of the transition regimes and the causes of differences between them is given in [5–10]. The nature of the N-regime of transition was elucidated both experimentally [5, 6] and theoretically (see reviews in [7–13]) soon after its first detection. As has been shown, the principal mechanism of the N-breakdown is related to the resonant parametric amplification of the background quasistochastic subharmonic disturbances due to their interaction with the primary instability wave. At the same time, progress in the understanding of the nature of K-breakdown has been rather slow over a long period of time. Now it is clear that the difficulties in this field were connected with the fact that the nature of the K-regime of boundary layer transition is significantly more complicated than that of the N-regime. The present paper is devoted to an experimental study of the K-regime of transition.

The structure of disturbances in the K-regime of the boundary layer breakdown was under intensive experimental study for thirty years (see [1–3, 14–18], for example). In particular, it has been shown in these works that the K-regime is characterized by the appearance, on the velocity oscilloscope traces, of powerful flashes of disturbances in the specific form of spikes with amplitudes up to 30–40 % of the potential flow velocity U_0. The nature of these flash-spikes and the cause of their appearance are the main problems in studying the K-breakdown process in the boundary layer. For many years their origin was associated with an "explosive" high-frequency secondary (usually local) instability of the flow and with the start of randomization of the laminar regime. Many of the difficulties in studying the K-breakdown were caused by the fact that in most experiments (starting with [3]) the study was based mainly on notions that were local in space and time, while in the theoretical works of the 1960s and 1970s spectral approaches were developed most intensively. In 1980, new detailed studies of the structure of the K-transition [19–21] were conducted on the basis of a unified spectral approach. The results of these experiments allowed one to obtain for the first time systematic information about both the frequency and frequency-wavelength structure of the disturbances, and led to a significant change in many notions about the character of the K-breakdown in the boundary layer. One of the important results of [19–21] was the conclusion that the flash-spikes are not stochastic but are strictly periodic structures generated as a result of gradual amplification of definite modes of the high-frequency spectrum and their phase synchronization.

Based on analysis of the experimental data of [5, 6, 19, 20], the theoretical results of [22–25], and some other works, a physical model of the initial stages of the K-regime of transition was suggested [7, 8]. It was termed the wave-resonant concept of breakdown. It was shown in [7, 8] that if the cascade of harmonic and parametric resonances between definite modes of the frequency-wavelength spectrum is actually realized, as was postulated within the framework of the concept, this leads to the appearance of flash-spikes (typical for

Institute of Theoretical and Applied Mechanics, Novosibirsk 630090. Translated from Prikladnaya Mekhanika i Tekhnicheskaya Fizika, Vol. 36, No. 4, pp. 60–97, July–August, 1995. Original article submitted August 22, 1994.

 0021-8944/95/3604-0532 $12.50

the K-regime of transition) which are concentrated exactly in those places in time and space where they are actually observed in experiments. The wave-resonant concept was justified further in [26, 27].

Further experimental study of the formation of the flash-spikes [28] allowed two main conclusions to be drawn: (a) generation of spikes is not connected with the mechanism of local inflectional high-frequency secondary instability of flow, as has been assumed for thirty years (see [29–32], for example); (b) spikes possess properties typical of solitons. The latter of these conclusions gave birth to new concepts of the mechanism of the K-regime of breakdown in the boundary layer.

The theoretical foundations for describing the soliton disturbances in the boundary layer were laid down in [33, 34], where the asymptotic theory based on the integral-differential Benjamin–Ono equation was developed. Although [33, 34] laid foundations for the subsequent mathematical description of the nonlinear stages of the K-regime of transition in the boundary layer, one can find therein no direct indication that their results can be used for explaining the nature of the flash-spikes.

The first attempt to use soliton solutions of the Benjamin–Ono equation for studying high-amplitude disturbances was made in [35]. However, the choice of a one-parameter family of solutions, considered therein, restricted the study to the analysis, most likely, of alternative or bypass ways of laminar-turbulent transition rather than of periodic regimes with spikes, characteristic of the K-regime of breakdown. Another approach was used in [36], where calculations of a two-dimensional wave packet were conducted within the framework of the theory of a boundary layer interacting with a triple-deck structure. The results obtained agreed very well with the observations in [28] and indicated the soliton behavior of the central cycles of oscillations within the packet where their amplitude became sufficiently high.

Further development of both experimental studies [37, 38] (see also [7, 8, 13, 39, 40]) and theory [41–43], and especially their unification in [42, 43] allowed the ultimate mathematically justified conclusion that the hypothesis suggested in [28] holds: "...the spikes observed in the K-regime of the transition... can be also considered as solitons" and "it is highly probable that the behavior of spikes... can be described within the framework of the theory of solitons."

In recent years, impressive advances in studying the nonlinear stages of transition, and, primarily, the K-regime of transition, were made on the basis of direct numerical simulation of flows in terms of the Navier–Stokes equations. It is impossible to describe within the scope of the present experimental paper the brilliant success of numerical methods used to study the occurrence of turbulence. These methods often demonstrate almost complete agreement with experimental results on transition [44–46]. The state of the art in studies devoted to this field is very well described in reviews [44, 47].

An experimental study of the final stages of the K-regime of transition and the causes of randomization of the flow was carried out in [48]. The results obtained indicate that the resonant interactions of instability waves of subharmonic type play a very important role in randomization of the laminar flow in both the K-regime and the N-regime of transition.

A detailed study of the properties of the flash-spikes arising in the K-regime of transition was conducted in the present work. These flash-spikes are, at least in the early stages of their development, the coherent structure-solitons (CS-solitons) of the transitional boundary layer (the term introduced in [39]). The field of other deterministic disturbances coherent with the fundamental wave, which arise and develop in the later stages of the K-regime of transition, has been studied, too.

2. Experimental Procedure. The experiments were conducted in a T-324 low-turbulence wind-tunnel at the Institute of Theoretical and Applied Mechanics of the Siberian Branch of the Russian Academy of Sciences at a flow speed of 9.18 m/sec and a turbulence level not exceeding 0.02%. [For convenience of comparison, the flow speed was chosen to be identical to that in the earlier series of experiments (see [19–21, 26–28], for example).] The tunnel has a 4-m-long test-section with a 1×1 m square cross section. The studies were conducted in a boundary layer of a flat Plexiglas plate which was 1.5 m long, 1 m wide, and 12 mm thick and positioned horizontally in the test-section of the wind-tunnel at a zero angle of attack. Under these conditions, a practically gradientless flow, corresponding to the Blazius boundary layer (as in [49, 50]), was formed over the plate surface (except for the vicinity of the leading edge).

In order to reproduce the K-regime of transition in a controllable way, initial disturbances were

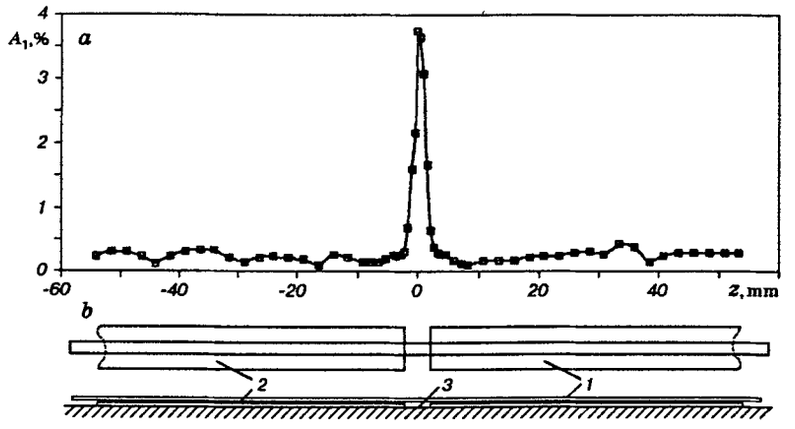

Fig. 1. Sketch of disturbance generator (b), consisting of vibrating ribbon (*1*) with pieces of adhesive tape (*2*) on the plate surface (*3*) and spanwise distribution of the amplitude of the fundamental wave (a), developing downstream the generator (x = 450 mm and $y = y_s$ = 3.0 mm.)

introduced into the boundary layer by means of a ribbon, oscillating at given frequency f_1, with pieces of an adhesive tape glued onto the surface of the plate under the ribbon. This disturbance generator was placed at a distance x = 250 mm downstream from the leading edge of the plate. A similar method was first employed in experiments [2], and then in a set of subsequent works (in particular, in [19–21, 28]). In contrast to previous studies, in the present work the pieces of the adhesive tape were not periodical along the span (i.e., along the z coordinate). Thus, they did not produce periodical spanwise modulation of the mean flow and disturbances but generated a solitary isolated peak (small knob initially) in the spanwise distribution of the amplitude of the primary quasi-two-dimensional fundamental instability wave introduced by the vibrating ribbon. This was achieved by using a piece of tape in the form of a continuous strip along the z coordinate, with a solitary opening in the vicinity of the point $z = 0$ (Fig. 1b).

Such a configuration of the piece of tape resulted in the appearance of a solitary (along z) region of formation of CS-solitons in contrast to the classical K-regime [19–21], wherein the spikes appeared at every period of spatial modulation in the region of peaks (i.e., of the local spanwise maxima of the disturbance amplitudes). The corresponding distribution of the amplitude of the fundamental wave A_1 (in percent of U_0) along the z-coordinate, obtained at x = 450 mm (in the stage of a developed spike), is given in Fig. 1a. The distribution was measured at a distance $y = y_s$ = 3.0 mm from the wall, where y_s corresponds to the maximum amplitude of the spike-soliton. The sharp peak on this graph corresponds to the region of formation of CS-solitons, which appears downstream the opening in the piece of tape (i.e., at $z = 0$).

All principal measurements were conducted with the use of a set of equipment based on a DISA 55M hot-wire anemometer with a linearizer. The probes were made of copper-plated platinum with a sensitive part 0.3 mm long and 6 μm in diameter. The data were recorded on an HO-62 seven-channel tape-recorder in the FM mode, followed by computer-based processing of the signals. The amplitudes of the velocity disturbances on oscilloscope traces, instantaneous profiles, and in Fig. 7a are given as instantaneous deviations from the mean values and in the other figures as the magnitudes of standard deviation. To measure phase relations, a reference signal, corresponding to the current through the vibrating ribbon (the source of instability waves), was recorded on one of the tape-recorder channels. Some details of the procedure of data processing are given below.

The frequency f_1 of the fundamental wave was chosen to be the same as in experiments [19–21, 26–28] and was equal to 96.4 Hz (the frequency parameter $F_1 = 2\pi\nu f_1/U_0^2 = 111 \cdot 10^{-6}$, where ν is the kinematic viscocity of the air, equal in this case to $1.55 \cdot 10^{-5}$ m^2/sec). The frequency of the signal discretization on

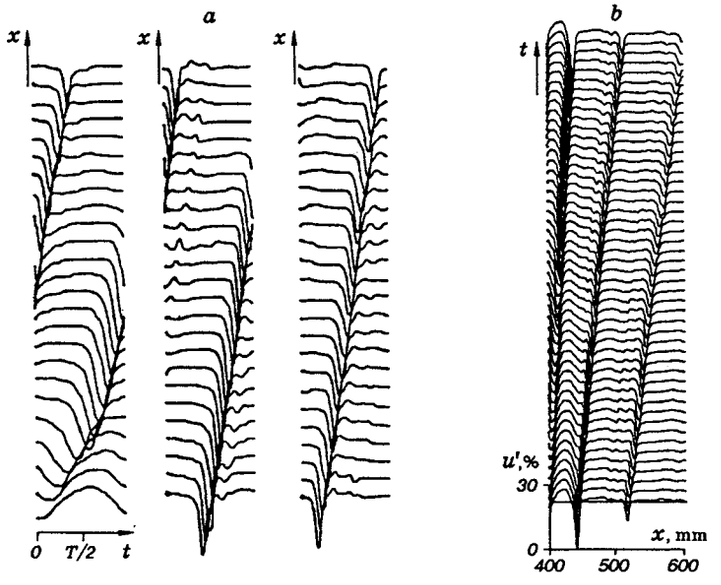

Fig. 2. Formation and downstream development of the spike-solitons. Fluctuations of the streamwise component of the flow velocity at $y = y_s(x)$ (see Fig. 3) and $z = 0$: (a) oscilloscope traces $u'(t)$ for various x; (b) spatial traces $u'(x)$ for various t (from $t = 0$ to $t = T$).

entering of the data into the computer corresponded to 48 points per fundamental period $T = 1/f_1$.

The main measurements were conducted in the range of magnitudes of the streamwise coordinate x from 300 to 800 mm (with the origin of coordinates at the leading edge), which corresponds, in an *undisturbed* laminar boundary layer, to local Reynolds numbers $\mathrm{Re} = U_0\delta_1/\nu$ (measured experimentally in [51, 52] and given in [50]) of 827 to 1272 (δ_1 is the boundary-layer displacement thickness). In the *disturbed* boundary layer, the local values of the displacement thickness δ_1 at points $x = 450$, 500, 550, and 600 mm in the vicinity of the peak of the amplitude of total fluctuations ($z = 0$), where most of the measurements were conducted, were equal to 1.66, 1.76, 1.53, and 1.60 mm, respectively, and the boundary layer thickness δ' [determined from $U(y) = 0.99U_0$] was 4.5, 7.0, 8.0, and 9.9 mm, respectively. In the later stages of the transition development, the local values of δ' were distorted noticeably by the presence of spike-solitons, which came to the external edge of the boundary layer (see Sec. 4). The boundary thickness δ, determined after subtraction of the local distortion (introduced into the mean velocity profile by spikes) was found to be approximately 4.5, 6.8, 7.4, and 8.8 mm at the same distances from the leading edge. For this reason, the local boundary layer thickness could be determined with much less precision than the displacement thickness δ_1.

The local Reynolds numbers were 982, 1041, 905, and 946 for $x = 450$, 500, 550, and 600 mm, respectively (at $z = 0$). Since the question of the characteristic local scale of the flow is unclear, most of the results of the present experiments are given below in dimensional coordinates.

3. Formation of Coherent Soliton-like Structures. Figure 2a shows a general pattern of formation and downstream development of localized coherent soliton-like structures associated with the "spikes" (spike-solitons), observed on the oscilloscope traces near the peak location (at $z = 0$).

The oscilloscope traces are shown in the region $x = 400$–595 (which is more than one hundred times larger than the boundary layer displacement thickness, equal to approximately 1.6 mm). The distance from the wall is different for each oscilloscope trace and corresponds to the amplitude maximum of the flash-spikes. The dependence of this distance, i.e., of the y-coordinate of the spike y_s, on the streamwise coordinate x is shown in Fig. 3. The oscilloscope traces were obtained after averaging an ensemble of 350 realizations of the periodic process with synchronization from the reference signal (i.e., from the current through the vibrating

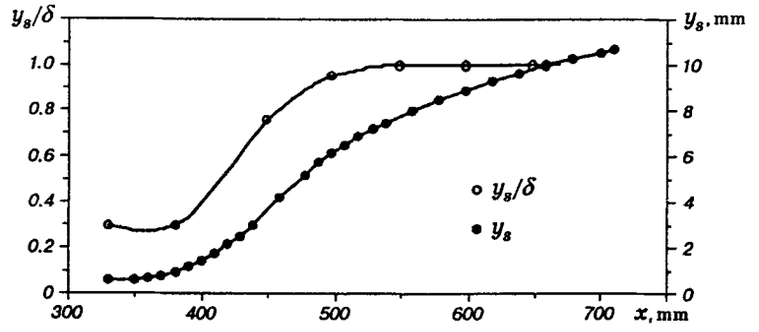

Fig. 3. Downstream evolution of the y-coordinate of the spike y_s, determined at the maximum point of its amplitude at $z = 0$.

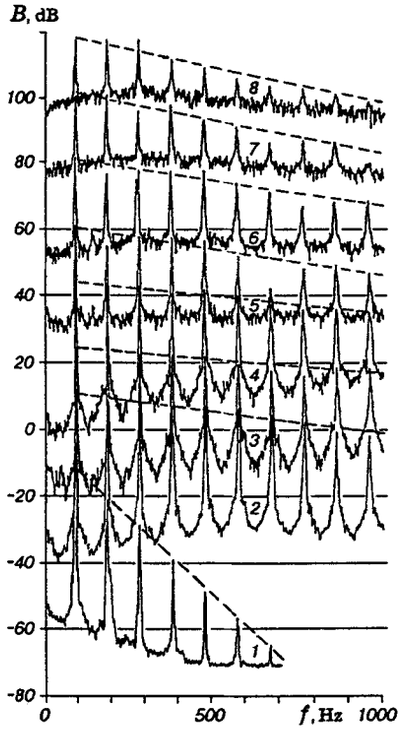

Fig. 4. Development of disturbance amplitude spectra obtained at $y = y_s(x)$ and $z = 0$: spectra *1–8* correspond to x = 400, 450, 510, 550, 610, 650, 710 and 770 mm (each successive spectrum is shifted by +20 dB).

ribbon).

The corresponding instantaneous profiles of velocity disturbance along the x-coordinate, determined for 48 moments of time (into which the fundamental period T was divided) are shown in Fig. 2b. The profiles ("spatial traces") demonstrate the process of formation and evolution of a spike-soliton in space.

Figure 2 shows first that the process of formation of coherent structures of this type is monotonous and regular, and second, that the structures retain their properties during downstream propagation, which is a characteristic feature of solitons. The amplitude spectra of disturbances shown in Fig. 4 adds to this picture. The spectra were obtained using an FAT-1 analog frequency analyzer with a bandwidth of 4 Hz. The oscilloscope traces taken were identical to those in Fig. 2 but without averaging over the ensemble. One can see that the disturbances during the process of their downstream propagation quickly form, at the stage from

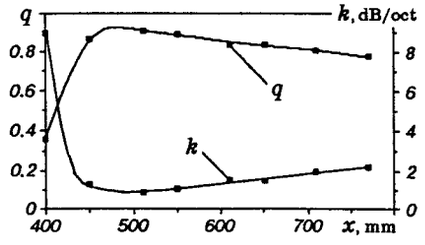

Fig. 5

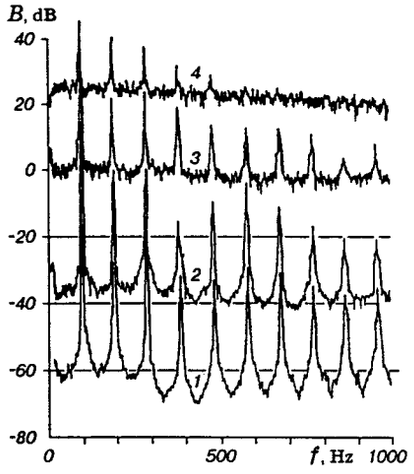

Fig. 6

Fig. 5. Evolution of the attenuation rate k of spectral harmonic amplitudes with frequency and corresponding values of the geometric progression factor q, determined from the spectra in Fig. 4.

Fig. 6. Onset of turbulence inside the boundary layer ($y \approx 2.0$ mm): amplitude spectra of disturbances *1–4* correspond to $x = 400$, 500, 550, and 600 mm at $z = 0$ (each successive spectrum is shifted by +20 dB).

$x = 400$ mm to $x = 450$–500 mm, a localized structure with the typical (essentially monotonous) attenuation of the harmonic amplitudes with frequency according to a geometric progression law. Such a behavior of the harmonics was first noticed in [7, 8] (and later in [28]) for initial stages of the spikes' formation. The corresponding dependences of the attenuation rate k of the harmonics' amplitudes and the progression factor q on the streamwise coordinate x are presented in Fig. 5. These values were determined for the late stages of spike-soliton formation by measuring the slopes of the envelopes shown by dashed lines in Fig. 4. A distinction of Fig. 5 from the corresponding graphs in [7, 8, 28] it that is was plotted on the basis of spectra measured at a distance of $y = y_s$ from the wall, i.e., along the trajectory of movement of the spike-soliton. The rapid decrease in the attenuation rate of harmonics with frequency, observed in the initial stage of formation of the structure, changes to a region where the shape of the deterministic part of the spectrum remains almost unchanged. The progression factor q reaches its maximum values (about 0.9) at $x \approx 500$ mm and then remains almost constant, decreasing very slowly to about ~ 0.78 at the end of the region of measurements.

The weak attenuation of the progression factor q after $x \approx 500$ mm (Fig. 5) is probably associated mainly with the gradual local transition of the flow to turbulence in the peak region ($z = 0$) initiated by deterministic disturbances. The transition leads to the beginning of a gradual (very slow) breakdown of the CS-soliton. The amplification of stochastic disturbances is readily seen in the spectra in Fig. 4. In the frequency range 300–400 Hz, for example, the level of turbulent fluctuations increases at the section from $x = 400$ mm to $x = 770$ mm by a factor of 100. However, the most intense growth of turbulence is observed not at the level of spikes, which "float" up toward the external edge of the boundary layer and move along it almost at $y_s = \delta$ [see the curve $y_s = y_s(x)$ in Fig. 3], but much closer to the wall. This fact is well illustrated by the spectra in Fig. 6 obtained at $y \approx 2$ mm (where the disturbances are most intense). In this region of the boundary layer, the intensity of continuous-spectrum fluctuations increases by a factor of 30 or 40 at a distance of only 150 mm, and the spectrum becomes very similar to the turbulent one even at $x = 600$ mm (i.e., at the stage corresponding to the final stages of the disturbance development shown in Fig. 2).

4. Downstream Evolution of Characteristics of Soliton Structures. The dependence of the quantities A_s and A_m, characterizing the amplitude of the spike (A_s is the maximum negative deviation of

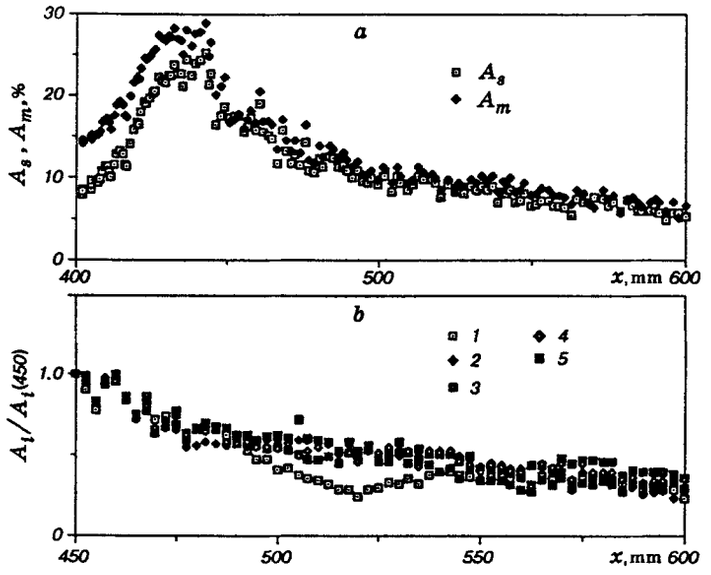

Fig. 7. Evolution of characteristics of spike's amplitudes A_s and A_m (a) and of normalized amplitudes of frequency harmonics (b): *1–5* amplitudes of harmonics with frequencies ω_1, ω_2, ω_3, ω_4, and ω_5; $y = y_s$; $z = 0$.

the instantaneous velocity from the mean value of the velocity, and A_m is the swing of oscillations of the flow velocity between the minimum and maximum values at the moment when the spike passes) is presented in Fig. 7a. The corresponding distributions of the normalized (by the values at point $x = 450$ mm) amplitudes of the fundamental wave and its four frequency harmonics are shown in Fig. 7b. It is very well seen from Fig. 7 that the amplitude of the spike exhibits nonmonotonous behavior in the stage of CS-soliton formation at $x \approx 400$–500 mm and reaches its maximum value at $x \approx 430$–440 mm. At the same time, the amplitude of the spike changes very slowly downstream, in the region where the formation of the soliton is finished (after $x \approx 500$ mm). In this stage of development, the spike comes to the external edge of the boundary layer and moves downstream along it (see Fig. 3).

It is seen from Fig. 7b that, after $x \approx 500$ mm, the attenuation rate of the spike's amplitude is approximately equal to that of the fundamental amplitude (with frequency f_1) and harmonic amplitudes (with frequencies $2f_1$–$5f_1$). This result agrees with Figs. 4 and 5, which demonstrate a similarity of the deterministic components of the disturbance spectrum observed after $x \approx 500$ mm. The spike's amplitude attenuates by a factor of two at a distance of approximately $75\,\delta_1$ (from $x = 490$ mm to $x = 610$ mm) in the region where a rather strong local (along z) turbulence of the flow appears. Then the attenuation rate becomes even lower. It should be noted that all higher harmonics of the fundamental wave (which form the spike) have to attenuate quickly according to the linear stability theory (see, for example, [50]) because they have very high frequencies which exceed significantly the frequencies of unstable disturbances (their frequency parameters $F_n = nF_1$, where n is the number of a frequency harmonic, and the wave $F_1 = 111 \cdot 10^{-6}$ lies within the region of the upper branch of the neutral stability curve when the Reynolds numbers are of the order of a thousand). However, no rapid attenuation of harmonics is observed in the nonlinear wave packet attributed to the spike-soliton. Probably, this property may be explained by the compensation of dissipativity by nonlinearity.

It was found in [19–21] that in the stage of formation of spikes their group velocity increases rapidly up to magnitudes close to the free-stream velocity, together with the phase velocities of the higher harmonics

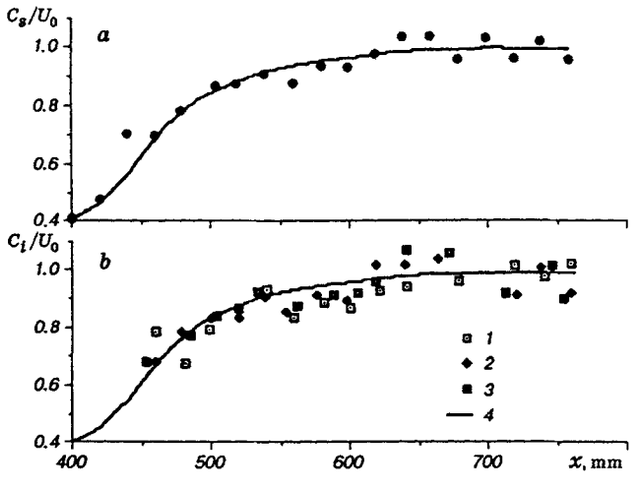

Fig. 8. Downstream evolution of the group velocity of a spike-soliton (points in a) and of phase velocities (b) of frequency harmonics ω_1, ω_2, and ω_3 (points *1–3*; line 4 is an approximation of the experimental points; $y = y_s$; $z = 0$).

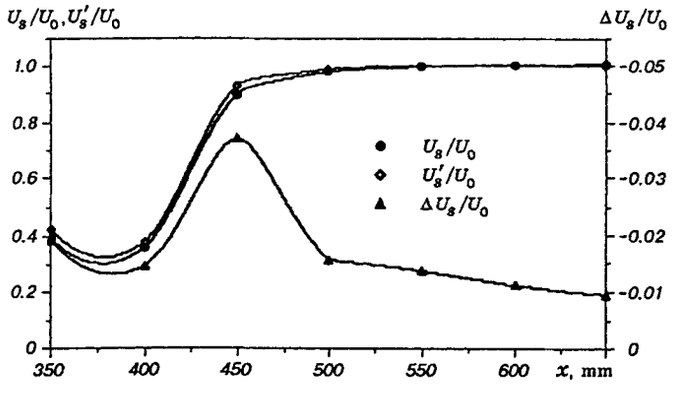

Fig. 9

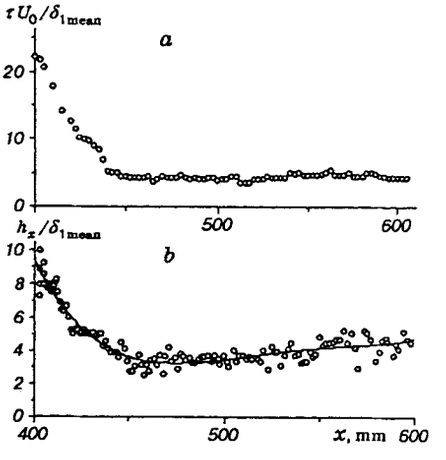

Fig. 10

Fig. 9. Dependence of the mean stream velocities U_s ($z = 0$), U_s' (averaged magnitudes for $z = \pm(5\text{–}10)$ mm), and of their difference $\Delta U_s = U_s - U_s'$; $y = y_s$.

Fig. 10. Onset of turbulence inside the boundary layer ($y \approx 2.0$ mm): amplitude spectra of disturbances *1–4* correspond to $x = 400$, 500, 550, and 600 mm at $z = 0$ (each successive spectrum is shifted by +20 dB).

(starting with the fourth one). The results shown in Fig. 8 supplement this observation for later stages of development of CS-solitons. The points in Fig. 8a correspond to the group velocity of the coherent structure as a wave packet, i.e., to the propagation velocity of the spike, and the line is an approximation of the experimental points. This line is plotted again in Fig. 8b, where the phase velocities of the primary wave and its second and third harmonics are presented. It is seen that the character of evolution of the group velocity is in good agrrement with the results of experiments [19–21]. At the same time, in the late stages of

development of a CS-soliton, in contrast to the stage of its formation, the phase velocities of all harmonics studied practically coincide with the group velocity of the soliton, at least when measured along the trajectory of the spike's movement (see Fig. 3), as has been done, in particular, in the case of Fig. 8.

Figure 9 demonstrates another curious property of coherent structures of this type. As mentioned earlier (see [2, 19–21], for example), the appearance of spikes is accompanied by a local decrease in the mean velocity of flow in comparison to the velocity at points neighboring along the spanwise z-coordinate. The dependence of this local defect (or "fall") of the mean velocity ΔU_s, caused by the presence of a spike-soliton and measured along the line $y = y_s$ (see Fig. 3), is shown in Fig. 9, where one can also see the values of the mean flow velocity in the vicinity of the spike: U_s at the point where the spike is located, U'_s at the points neighboring along z and having the same x and y coordinates ($\Delta U_s = U_s - U'_s$ by definition). Again it is seen that the coordinate $x \approx 500$ mm may be regarded as the place where the formation of the spike-soliton is completed, and, starting with this coordinate, one can say that the CS-soliton is fully developed. Downstream, the defect of the mean velocity ΔU_s, as well as other parameters of the soliton, changes very slowly.

Finally, let us consider one more characteristic of spikes as wave packets, namely, the rate of their spread in time (and along the x-coordinate). The downstream evolution of the temporal length of the spike τ, determined at the one-half level of its height, is shown in Fig. 10a in the dimensionless units $\tau U_0/\delta_1$ (calculated for the mean value of the displacement thickness $\delta_{1\text{mean}} = 1.66$ mm). The corresponding evolution of the spatial (along the x-axis) width of the spike is shown in Fig. 10b. It is seen that after the formation of the CS-soliton and the process of its localization ("self-focusing") have been completed, the characteristic size of the structure along both x and t becomes very small. For example, if $x = 500$ mm, then $\tau \approx 0.83$ msec, $\tau/T \approx 0.08$ (T is the period of the primary wave), and $h_x \approx 6$ mm, and $h_x/\lambda_{sx} \approx 0.08$ (λ_{sx} is the distance between the spikes along x and the width h_x was determined from the data presented in Fig. 2b). These sizes remain virtually unchanged further downstream, despite the significant dispersion existing for linear instability waves (and for the linear wave-packets).

5. Structure of Disturbances in Physical and Fourier Spaces. The above results were obtained mainly in the plane of the soliton's formation, i.e., at $z = 0$. The results of measurements presented below demonstrate the three-dimensional structure of CS-solitons in the boundary layer.

5.1. *Dependence of the disturbance characteristics on the spanwise coordinate.* Figure 11 presents the families of instantaneous profiles of disturbances of the flow velocities obtained for three values of the x-coordinate from the ensemble averaged families of oscilloscope traces measured at distances from the wall that correspond to the maximum amplitude of the spike $y = y_s$ (see Fig. 3). The figure visually demonstrates the spatial form of the spike-soliton, and, in particular, its strong localization along the spanwise coordinate z. This peculiarity is an inherent property of the studied type of coherent structures in the late stages of their development (in this case, after $x \approx 500$ mm). The spike-soliton (in the region $y = y_s \approx \delta$) is seen to be a strongly pronounced peak with a small typical "tail" of quasiharmonic oscillations that attenuate quickly as the t- (or x-) coordinate increases. Note that in view of conservation of the CS-soliton's properties, its small typical size along the x-axis, and the weak gradient $\partial U/\partial y$ in the region of spike localization, the disturbances are, in fact, "frozen," and the t-coordinate is practically equivalent to the coordinate $x = -C_s t$, where the disturbance propagation velocity C_s is approximately equal to U_0. Starting with $x \approx 500$ mm, the characteristic size of the peak along the z-axis changes very slowly as the peak moves downstream. Figure 11 also shows that in the latest stages (when $x \approx 600$–650) the flow in the vicinity of the CS-soliton is already strongly disturbed by transition of the flow to turbulence occurring there (mainly near the wall and inside the boundary layer). This, however, does not lead to any significant changes in the shape and size of the main peak.

Figure 12 shows the spatial distributions of other characteristics of CS-solitons, namely, of the amplitude of spikes A_s, the amplitude of the fundamental wave A_1, and the defect of the local average flow velocity ΔU_s, obtained at $y = y_s$ and normalized by their maxima. The plots show quantitatively the severe spanwise localization of the soliton, its characteristic size along the z-axis being ($x \approx 500$ mm), $h_z \approx 4$ mm (i.e., $h_z/\delta_1 \approx 2.3$) in this stage of development. It is seen from Fig. 12 that these three distributions are

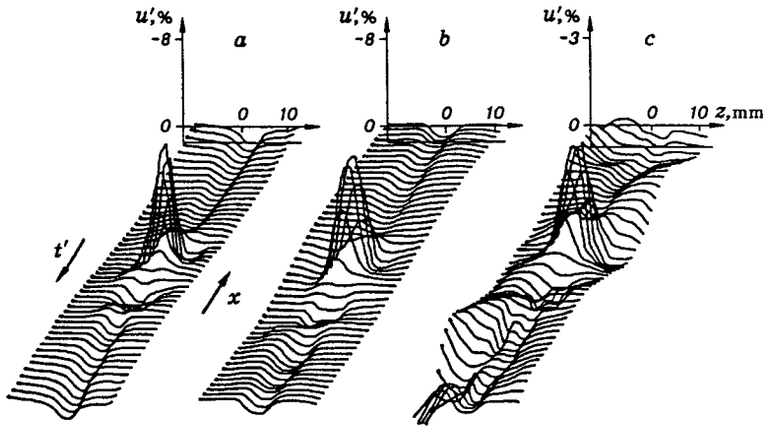

Fig. 11. Shape of spike-soliton in the (t, z) or (x, z)-plane at $y = y_s$. Instantaneous profiles of the velocity disturbance u' along z at $x =$ 500, 550, and 650 mm (a–c).

similar in shape. In this connection, each of these distribution can quantitatively characterize the spatial size and shape of the soliton.

The spanwise distributions of the fundamental wave amplitude, obtained at various downstream positions and shown in Fig. 13, demonstrate how the spatial form of CS-solitons evolves starting with the early stages of its development. It is seen that the spatial localization of the soliton (self-focusing along the z-axis) occurs in the stage of its formation. Such behavior of the disturbance is contrary to the usual spreading typical for linear packets of instability waves [51, 52]. Starting with $x \approx 500$ mm, the characteristic width h_z of the soliton becomes almost constant.

5.2. *Spectral characteristics of disturbances.* Fourier analysis of the disturbance field, conducted in any studies, has two meanings. First, there is a kinematic (or geometric) meaning, and second, a dynamic (or physical) one. In the kinematic aspect, the Fourier analysis makes it possibile to study the shape of the spatial and temporal distributions of parameters characterizing the disturbance from the spectral standpoint. In the dynamic aspect, this analysis provides information about the laws of development and interaction of spectral modes in the Fourier space. If one uses a very simplified three-grade scale (0 — insignificant, 1 — meaningful, and 2 — very significant) to evaluate the significance of both aspects of the Fourier analysis for the problem of transition, then different stages of the process of turbulence onset can be associated with the values of the "significance vector" $\mathbf{S} = (S_k, S_d)$ in a two-dimensional space of the above aspects of the Fourier analysis (S_k is the kinematic significance and S_d is the dynamic one). For the linear stages of development of instability waves, $\mathbf{S}_L = (0.2)$, for the weak nonlinear stages, $\mathbf{S}_w = (1.1)$, and for the strongly nonlinear stages, $\mathbf{S}_N = (2.0)$.

Indeed, in the linear region, the form of any packets of instability waves is entirely determined by the properties of the disturbance source and the superposition of independently developing spectral modes (see [51, 52], for example). Hence, there is no physical sense in describing this form geometrically ($S_{kL} = 0$). At the same time, the Fourier analysis is a powerful and unique tool for describing the processes of development of small disturbances by means of their decomposition into normal harmonic modes. In the dynamic sense, there is a close connection between oscillations at any two points of the physical space, while any two modes in the Fourier space are totally independent of each other ($S_{dL} = 2$).

In the weakly nonlinear region, the complete independence of the spectral modes disappears and weak nonlinear interactions between them come into play (initially, interactions of pairs and triads, then interactions of higher order). As the amplitude grows, the dynamic description of the process of disturbance evolution with the aid of the spectral approach becomes more and more complicated, and this approach gradually loses its advantages over the description using the physical space (i.e., $S_{dw} = 1$). At the same time, in the

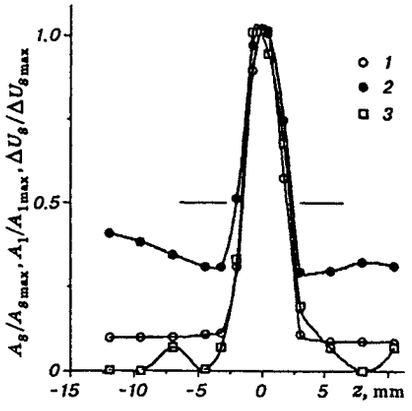

Fig. 12

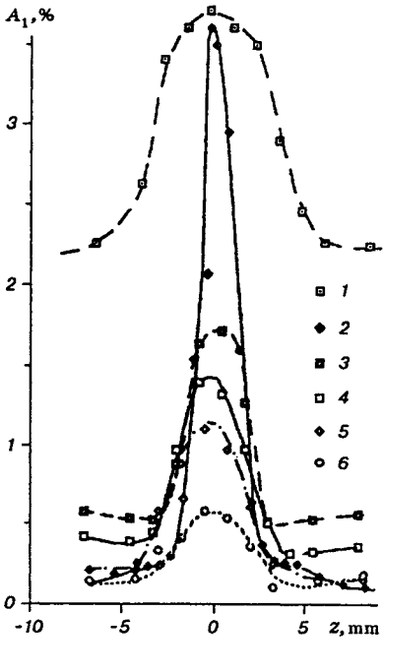

Fig. 13

Fig. 12. Normalized spanwise distribution of amplitudes of the spike A_s, the fundamental wave A_1, and the defect ΔU_s in the mean velocity profile (points *1–3*) at $y = y_s$ and $x = 500$ mm.

Fig. 13. Self-focusing of spike-soliton along the spanwise coordinate. Distributions of the fundamental wave amplitude A_1 at $y = y_s$: *1–6* correspond to $x = 380$, 450, 500, 550, 600, and 650 mm.

physical space, some "geometric" formations appear in the weak nonlinear stages (e.g., Λ-structures, coherent structures, etc.). They consist of spectral modes that have relatively stronger (resonant) connections. A kinematic description of these structures gives certain weight to the geometric aspect of the spectral approach ($S_{kw} = 1$).

In the stages of strong nonlinear disturbance development (if such are realized), the dynamic sense of the Fourier analysis practically comes to naught ($S_{dN} = 0$), because the interacting spectral modes can strongly influence one another and the number of the determining degrees of freedom (the actual dimensions of the physical system) is not only unable to decrease when changing to a Fourier space, but, on the contrary, can increase. At the same time, in the physical space some strong-nonlinear, strongly localized structures (quasi-particles) can appear which have some stable kinematic (geometric) characteristics. A description of these characteristics using spectral methods is of great importance for their identification and for the study of their evolution ($S_{kN} = 2$).

In connection with the preceding, the spectral analysis of the disturbance field is of great interest in all stages of the transition development, though in different stages the reasons for this interest are different.

The distributions of the amplitudes and phases of a set of higher-frequency harmonics (as well as of the primary wave) along the spatial z-coordinate for successive values of the x-coordinate are shown in Fig. 14(a–d). The amplitude profiles are very similar in shape for all the harmonics. This shape resembles a narrow peak along the z-coordinate. The characteristic width of the peak is practically the same for all harmonics at every fixed value of the x-coordinate and increases very slowly downstream (as x grows). The similarity in shape of the profiles of higher harmonics is clearly seen in Fig. 14e, where the distributions corresponding to Fig. 14b and normalized by their maximum values are presented.

The z-distributions of the phases φ_i' of harmonics [Fig. 14(a–d)] indicate the high degree of phase

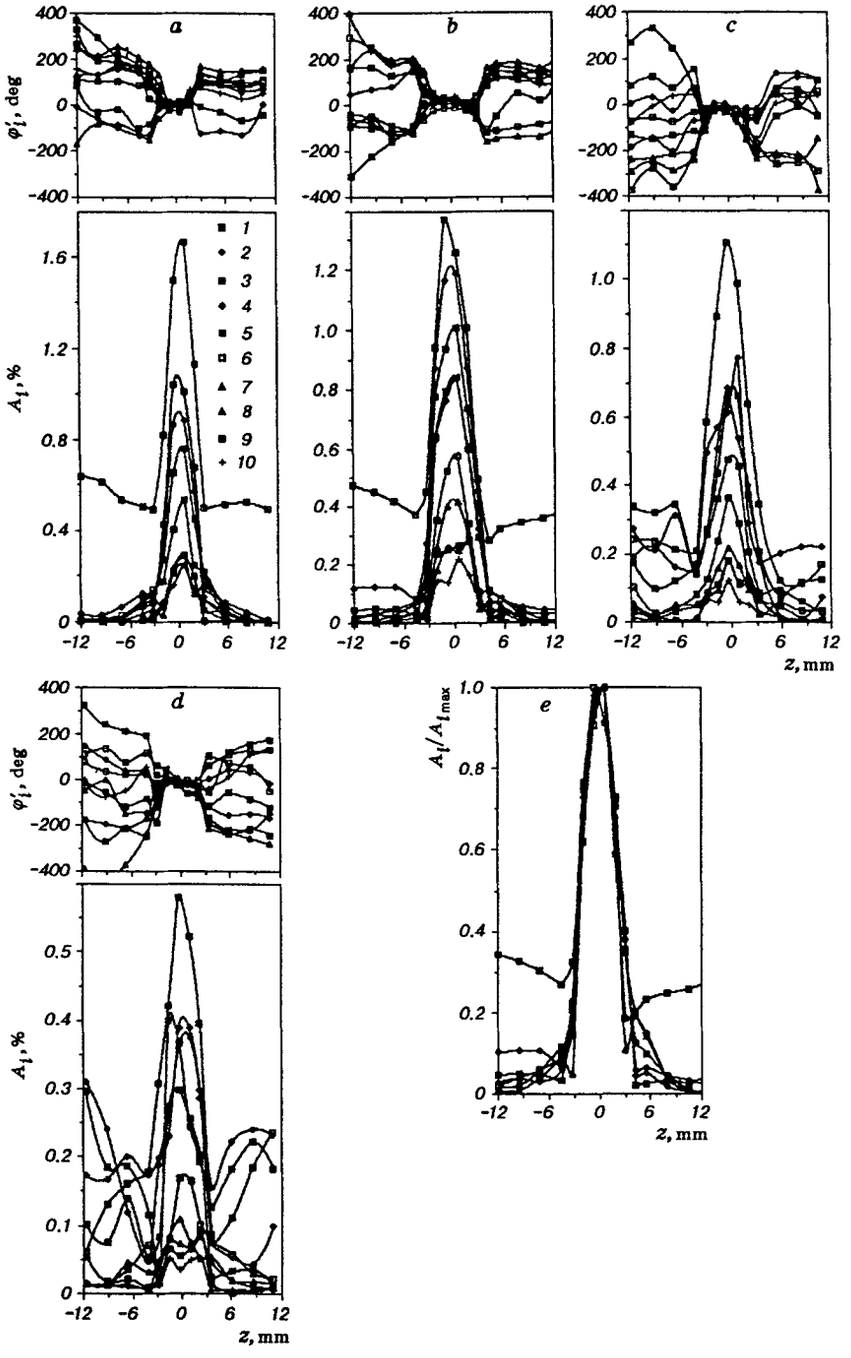

Fig. 14. Spanwise dependences of amplitudes A_i and phases φ_i' of frequency harmonics ω_i on z at $x = 500$, 550, 600, and 650 mm (a–d) and comparison of the normalized distributions for the amplitudes $A_i/A_{\max}$ at $x = 550$ mm (e): *1–10* correspond to $\omega_1, \ldots, \omega_{10}$; $y = y_s$.

synchronization in the frequency spectrum observed inside the spike-soliton. The phases φ_i' correspond to the phases of the wave valleys but not to their crests, namely, they are the places of oscillations of type $-A_n \cos(n\omega_1 t)$, counted off from the time moment that corresponds to the spike's peak, i.e., to the minimum of instantaneous velocity in the structure observed on the oscilloscope traces at $z = 0$.

The profiles of the amplitudes and phases in Fig. 14 correlate very well with the corresponding

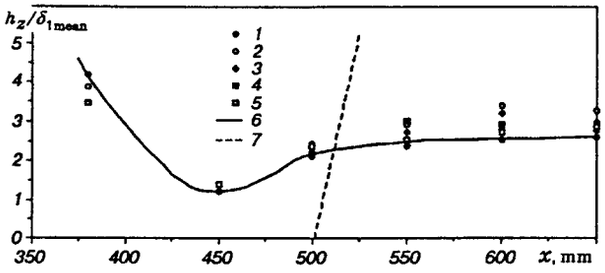

Fig. 15. Downstream dependence of the spanwise size h_z of the spike-soliton determined from the amplitude of the spike, amplitude of the harmonics ω_1, ω_2, and ω_3, and from the defect in the mean velocity profile (points *1–5*); *6* is an approximation of points *1*; *7* is the spreading rate of the linear packet [27]; $y = y_s$.

distributions measured in [19–21] for the initial stages of formation of spikes and termed there the "spikes in space." A comparison shows that the main properties of these distributions are practically the same in all stages of the development of CS-solitons, starting with the stage of the spike appearance, i.e., the case of periodic peak regions along z in [19–21] differs little from the case of an isolated peak region, realized in the present work.

On the whole, the distributions given in Fig. 14 show the conservative behavior of the spectral content of the soliton coherent structure in the frequency spectrum. This behavior is observed in the essentially three-dimensional stages of the development of the structure.

Some quantitative characteristics of the spanwise dispersion of the CS-soliton are shown in Fig. 15. Its characteristic spanwise width h_z was determined from the distributions in Figs. 12–14 at the one-half level of the maximum value (see the two horizontal dashes in Fig. 12) for each of the measured characteristics, i.e., from the z-distributions: *1* of the amplitude of the spike; *2–4* of the amplitude of the primary, second, and third harmonics, *5* of the defect of the mean flow velocity at the location of the structure. It is seen from Fig. 15 that all the methods for determining the dependence $h_z(x)$ yield practically the same rate of the spanwise spreading of the soliton, as it moves downstream, and close values of its spanwise width. At the stage of formation (i.e., approximately at $380 \leqslant x \leqslant 500$), a rapid self-focusing of the structure and small inverse relaxation are observed. After that, the soliton moves downstream almost without any spanwise spreading. The typical angle of its spreading in the (x, z) plane, in stages after $x \approx 500$ mm, is as small as about 0.2°, which is 45 times less than the corresponding angle for a linear wave packet with low amplitude (generated by a point source), which was measured at the same free-stream velocity and frequency of the fundamental wave [51, 52] and was found to be approximately 9.0°. This "linear" angle is shown in Fig. 15 in a dashed line.

It is clear that the spanwise spreading of the linear packet is mainly connected with two circumstances: the dependence of the phase velocities of the three-dimensional instability waves on their propagation angle, and the rapid attenuation in the linear case of three-dimensional waves inclined at large angles with respect to the flow direction [50–52]. Nonlinearity in the CS-soliton compensates the dispersion (along t, x, and z) and leads to the properties of the soliton being constant for long distances downstream, which range up to tens of the characteristic size of the soliton and more than a hundred displacement thicknesses of the boundary layer. From Figs. 12–15, one can draw a general conclusion that, for all the measured distributions (at $y = y_s$) and in all stages of development (after the formation process is completed), the z-distributions of the amplitudes of harmonics that form the spike-soliton predominantly have the shape of a peak with pronounced maximum, the location of which coincides with the center of the soliton ($z = 0$), and its shape remains practically unchanged, as shown by the wave spectra.

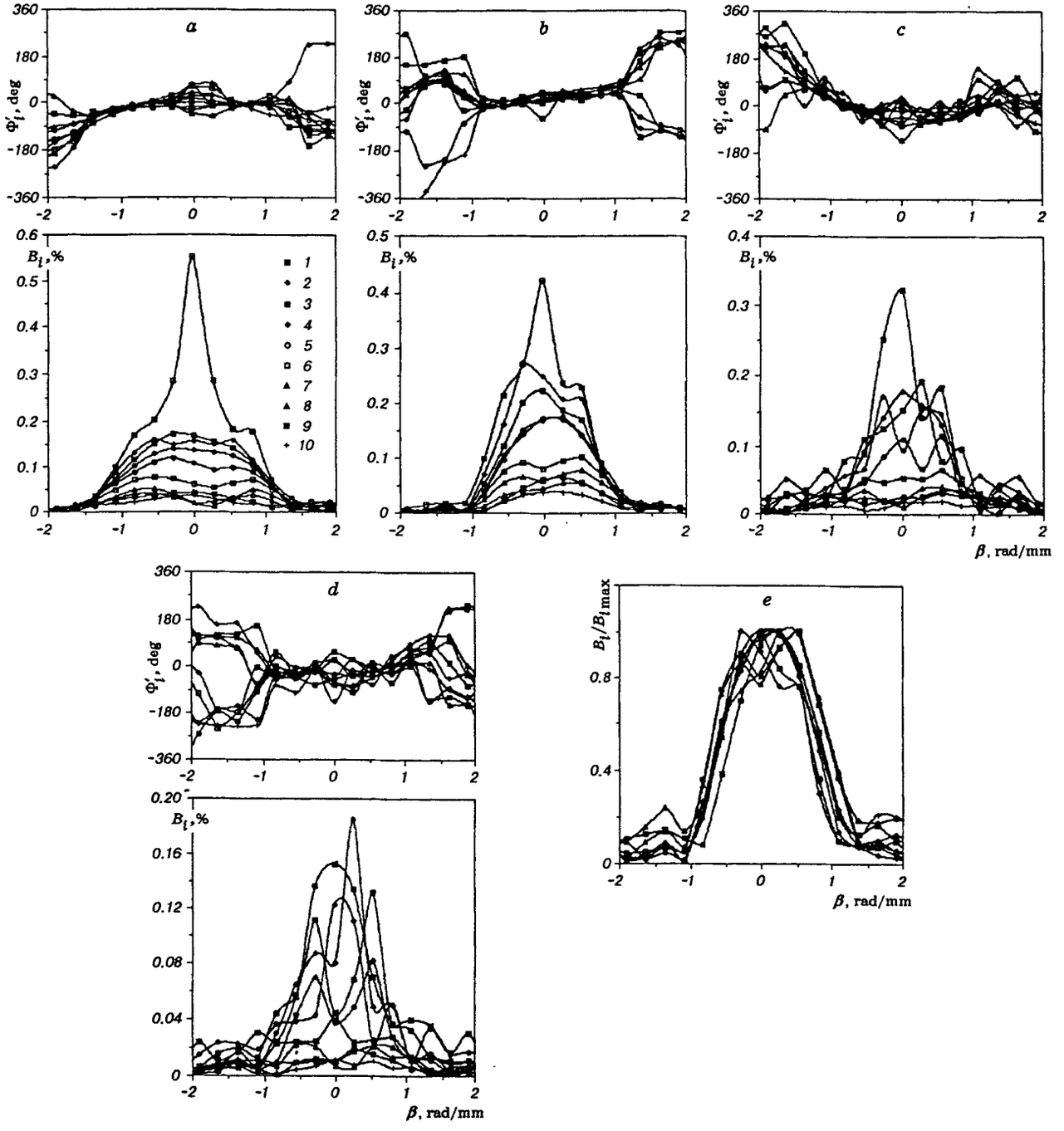

Fig. 16. Amplitude and phase parts of the wavenumber spectra of the spike-soliton at $x = 500$, 550, 600, and 650 mm (a–d), and normalized amplitude wavenumber spectra at $x = 550$ mm (e): *1–10* correspond to $\omega_1, \ldots, \omega_{10}$; $y = y_s$.

In view of the essentially three-dimensional nature of a CS-soliton, it is interesting to study its frequency-wavenumber spectrum after performing the double Fourier transform along the coordinates t and z.

The results of wave analysis of the distributions given in Fig. 14a–d for the late stages of development (from $x = 500$ mm to $x = 650$ mm) under the conditions of the present experiments are shown in Fig. 16 in

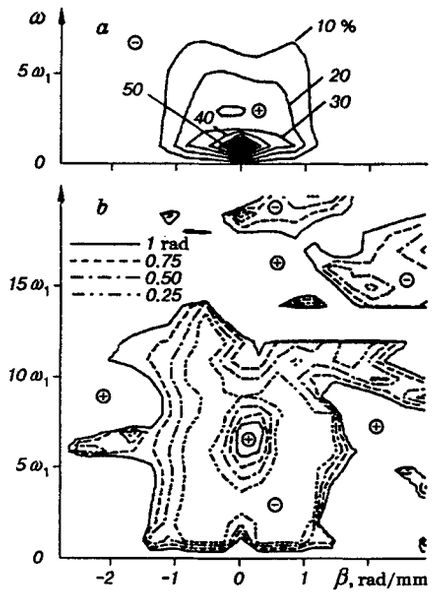

Fig. 17. Contours of the amplitudes (a) and the module of phases (b) of the modes of the spike-soliton's frequency-wavenumber spectrum at $y = y_s$: the spacing between amplitude contours is 10% of $B_{i\,\max}$ (in the range from 100 to 10%); the spacing between the phase contours is 0.25 rad (in the range from 1 to 0.25 rad); $x = 500$ mm.

the form of sections of the frequency-wavenumber spectra along $\omega =$ const (for different values of $\omega = n\omega_1$, $n = 1, 2, 3, \ldots$) as functions of the spanwise wavenumber β.

The amplitude wavenumber spectra demonstrate the predominance of a plane wave ($\beta = 0$) at the frequency of the fundamental harmonic in almost all stages of development. The plane wave of oscillations at the frequency of the fundamental wave ω_1 always surpasses any of the three-dimensional modes ($\beta \neq 0$) in amplitude. As for the remaining harmonics, modes with $\beta = 0$ are not pronounced in the spectrum, as a rule. Similar to the case of the fundamental wave ω_1, most distributions for higher-frequency harmonics are almost symmetric with respect to the axis $\beta = 0$. Maximum amplitudes are achieved either at $\beta \approx 0$ or at $\beta \approx \pm\beta^*$, where the values of β^* range from 0 to approximately 0.8 rad/mm ($\beta^*\delta_1$ ranges from 0 to 1.4, correspondingly). (It seems plausible that the existing asymmetry is merely due to the error of measurement which grows with frequency and the x-coordinate.) The region of the frequency-wavenumber spectrum that contains the most energy of oscillations is located mainly in the range of wavenumbers $\beta \approx \pm 1$ (i.e., $\beta\delta_1 \approx \pm 1.7$). This value corresponds to a characteristic spatial size of the spike-soliton of about 6 mm (i.e., about $3.5\delta_1$). As seen from Fig. 16e, the shape of the amplitude spectra for the modes ω_2, ω_3, $\omega_4 \ldots$ is self-similar (within the limits of some experimental spread).

The corresponding phase spectra (Fig. 16) demonstrate synchronization of phases of the frequency-wavenumber harmonics Φ' in a wide range of frequencies (from $\omega = \omega_1$ to $\omega = (10\text{–}12)\omega_1$)) and wavenumbers (from $\beta \approx -1$ rad/mm to $\beta \approx +1$ rad/mm or from $\beta\delta_1 \approx -1.7$ to $\beta\delta_1 \approx +1.7$). Plane modes ($\beta = 0$) which are synchronized noticeably worse than three-dimensional modes are an exception in the wave spectrum. The best synchronization of the modes is observed at $x = 550$ mm, where the soliton appears to be fully formed and turbulence fluctuations in the flow, which destroy the phase synchronization, are not too strong yet. At the last measured section ($x = 650$ mm), the accuracy of synchronization is markedly diminished and the

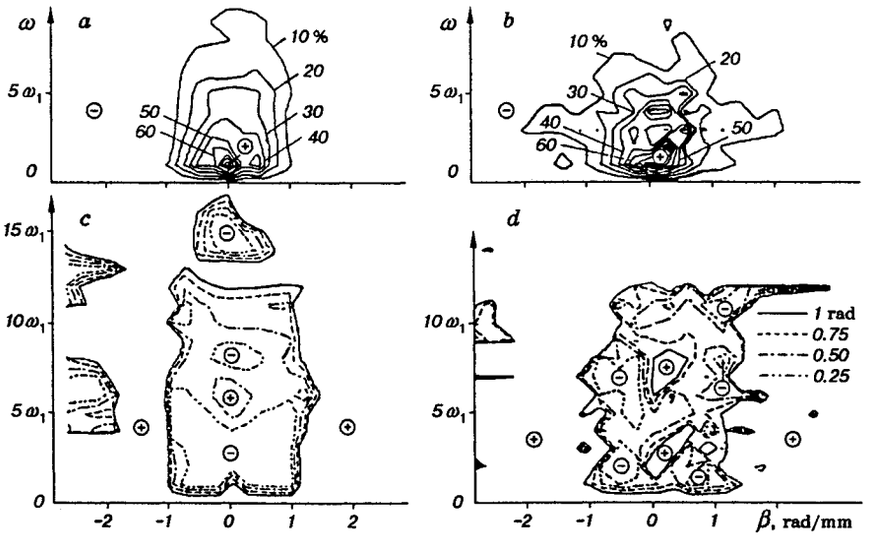

Fig. 18. See Fig. 17 for caption; $x = 550$ (a and c) and 650 mm (b and d); a and b are amplitude spectra; c and d are phase spectra.

range of wavenumbers within which synchronization is observed becomes somewhat narrower. These features are, in all appearance, associated with a strong noise (including the phase one) introduced by the turbulence that develops inside the boundary layer.

In [19–21], it was first shown that the modes of the frequency-wavenumber spectrum (for the successive frequencies ω_1, $2\omega_1$, and $3\omega_1$) have some zones of phase synchronization occurring at $x \approx 430$ mm at the moment when the first spike is formed on the oscilloscope traces. The spectra shown in Fig. 16 are in good qualitative agreement with the results of [19–21] and show that the structure of frequency-wavenumber spectra (both of phase and amplitude ones) remains qualitatively unchanged in all stages of the development of CS-solitons and is characterized by a set of frequency-wavenumber harmonics with typical wavenumbers $\beta\delta_1$ of order ± 1 (up to $\sim \pm 1.7$), which are synchronized with one another in places.

The above-mentioned zones of phase synchronization are most pronounced in the two-dimensional (ω, β) distributions of the amplitudes B_i and phases Φ_i of the frequency-wavenumber modes shown as isolines in Figs. 17 and 18. Figure 17 corresponds to the x-coordinate where a three-dimensional soliton is almost formed and Fig. 18 shows the subsequent stages of its development. The amplitude parts of the frequency-wavenumber spectra (Figs. 17a and 18a, b) clearly demonstrate that the main energy of disturbances within the soliton is concentrated inside a nearly rectangular region, the borders of which (at the 10% level of the maximum amplitude) are outlined by the lines $\beta \approx \pm 1$ rad/mm ($\beta\delta_1 = \pm 1.7$), $\omega = 0$, and $\omega \approx 7\omega_1$. Strong phase synchronization of frequency-wavenumber modes is observed in the phase parts of spectra (Fig. 17b, 18c, d) inside a region of approximately the same rectangular shape and with the same width along the axis of the wavenumbers β. Though the length of this region along the frequency axis is markedly greater than that of the zone of amplitudes, exceeding 10% percent of the maximum, it extends approximately up to frequencies $\omega \approx 12\omega_1$.

The region of phase synchronization of the modes (with $|\Phi'| \approx 0$) resembles a "pit" with precipitous edges and an almost flat bottom. The steepness of the edges (i.e., the density of the phase isolines) grows somewhat at the section from $x = 500$ mm to $x = 650$ mm).

In the last studied point ($x = 650$ mm) the edges of the synchronization zone become indented and slightly blurred with turbulence. There are some "hillocks" on the bottom of the "pit" (observed near $\beta = 0$) which correspond to zones of worse synchronization. The location of these "hillocks" of desynchronization along the ω-axis and their height depend on the x-coordinate. It is interesting to note that one of the "hillocks" emerges on the lower edge of the "pit" and its center coincides, for all x, with a plane fundamental wave that

is not synchronized with the soliton.

Thus, the above characteristic of the shape of spike-solitons in the physical space, as well as in the frequency and frequency-wavenumber spectra, demonstrate their rather simple and regular structure which, like some other properties of the CS-solitons remains almost unchanged for a long distance downstream up to the final stages of the laminar-turbulent transition.

6. Normal-to-wall Structure of Disturbances. 6.1. *Initial stage of development of a CS-soliton.* The structure of disturbances along the normal-to-wall coordinate y, corresponding to the initial stage of development of a CS-soliton ($x = 450$ mm), is illustrated in Figs. 19–21, where a comparison is given with the data of [28].

Five families of velocity oscilloscope traces, obtained during displacement of the probe away from the wall, are shown in Fig. 19. Three of them are: (a) single realizations of the process, (b) traces averaged over 350 periods and representing the periodic component of fluctuations, and d) filtrated high-frequency ($\omega \geqslant 6\omega_1$) traces obtained from Fig. 19b and denoted H_6 in [28]. Figures 19 b, d are taken from [28] at $x = 440$ mm and correspond to Figs. 19c, e in the present experiments.

Figure 20 presents three types of instantaneous velocity profiles obtained by passing a section through data arrays along the planes $t =$ const. The instantaneous profiles in Figs. 20a, d show the total flow velocity (denoted M_Σ, as in [28]) and profiles in Figs. 20b, c, e, f represent the low-frequency part of the instantaneous velocity. The profiles in Figs. 20b, e are formed only by the mean velocity and the disturbances with frequencies $\omega \leqslant 3\omega_1$ (denoted M_3 as in [28]), while the profiles in Figs. 20c, f are formed only by the mean flow velocity and the fundamental wave with frequency ω_1 only (the profiles M_1). Figures 20d–f are plotted on the basis of the data from [28] and are given for comparison.

At $x = 450$ mm, the flow remains practically periodical in time, which is evidenced, in particular, by the almost complete similarity between the averaged (Fig. 19b) and nonaveraged (Fig. 19a) oscilloscope traces. The amplitude of flash-spikes there is close to their maximum values. At $y \approx 2.8$ mm ($y/\delta \approx 0.62$), it reaches $\sim 30\,\%$ of the mean free-stream velocity (cf. Fig. 7a) and $\sim 40\,\%$ of the local mean flow velocity. The typical sharp spikes on the oscilloscope traces are observed approximately at $0.62 \leqslant y \leqslant 0.76$. The traces H_6 (Fig. 19d) show that almost the whole high-frequency part of fluctuations is concentrated within the middle part of the boundary layer (approximately at $0.47 \leqslant y/\delta \leqslant 0.76$), where the spike-solitons are formed. This agrees very well with the results of the asymptotic theory (see [41–43]), where the spike-solitons described by the Benjamin–Ono equation develop in the so-called intermediate sublayer located in the interior of the boundary layer. The thickness of this sublayer is rather large and increases with increasing amplitude of the soliton, whereas no solitons are observed in the near-wall region and in the outer part of the boundary layer in the stage described by this theory (see below).

In the stage under study, the instantaneous flow velocity profiles remain rather filled and close to the profile of the undisturbed boundary layer during the greater part of the period. The region of strongly disturbed instantaneous profiles (Fig. 20a at $t' \approx T/2$) coincides approximately, in this stage of development, with the region of formation of spike-solitons observed on the oscilloscope traces (Fig. 19a, b). In essence, the instantaneous profiles in Fig. 20a and averaged oscilloscope traces in Fig. 19b are two families of sections (along $y =$ const and $t =$ const, respectively) of the same array of experimental data and reflect two viewpoints on forming the CS-soliton.

A strong high-shear layer (HS-layer) exists in the instantaneous profiles M_Σ (Fig. 20a) during a period of time from approximately the 19th to the 39th profile. At this stage it is located approximately at $0.3 \leqslant y \leqslant 0.6$. The regions along t and y where both the HS-layer and solitons exist overlap (the spike corresponds to the profile 24 in Fig. 20a); however, the centers of these regions do not coincide, especially along the y-coordinate. These regions have a tendency to diverge as the spike-soliton develops. This tendency increases downstream and leads to almost total separation of the regions along t and y as early as at $x = 500$ mm. This separation of disturbances into two types was thoroughly studied in [28] in connection with the investigation of the role that the mechanism of local high-frequency secondary instability of flow plays in the process of generation of flash-spikes. The data obtained in the present paper reproduce adequately the results of [28] and extend them to the later stages of development of CS-solitons. At the same time, there are certain distinctions which

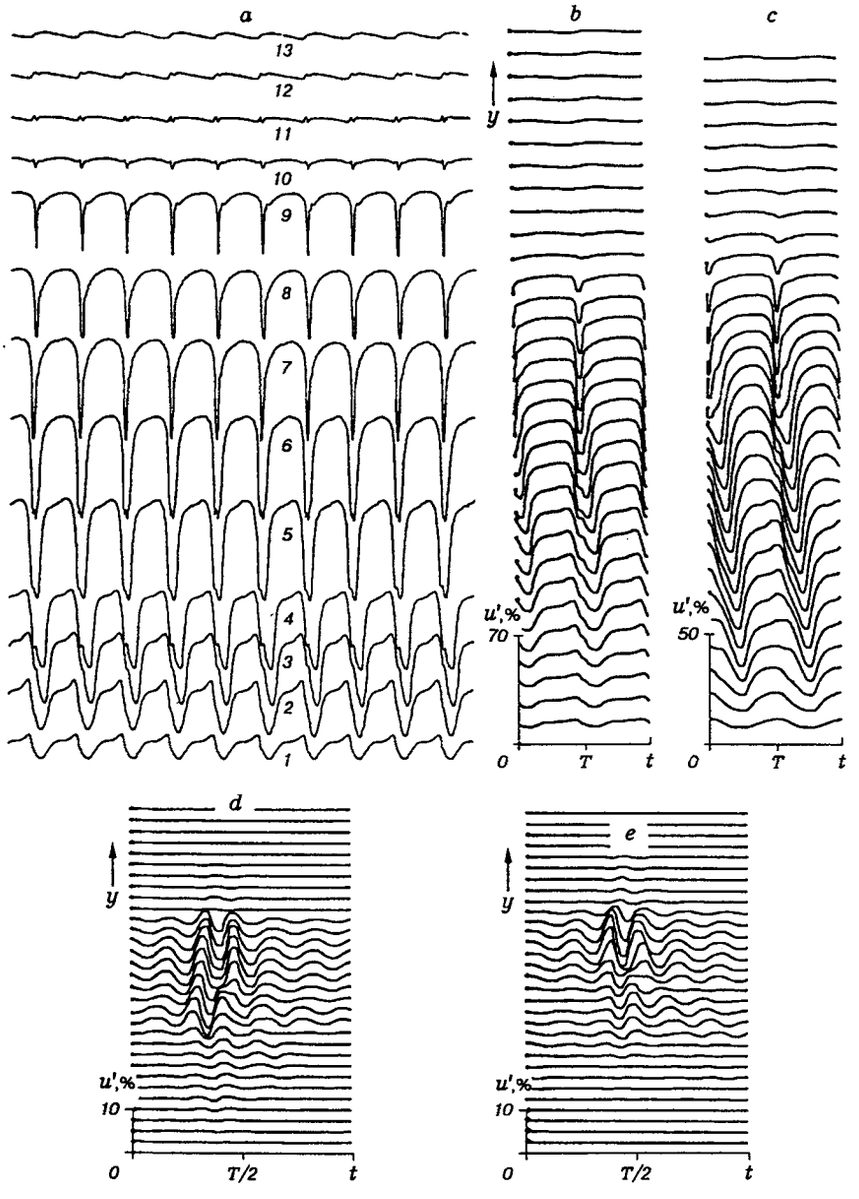

Fig. 19. Traces of velocity fluctuations (synchronized with the reference signal) obtained at different distances from the wall at $x = 450$ mm (a, b, and d) in the present work and at $x = 650$ mm (c and e) in [28]: a is hot-wire signal; b and c are synchronously averaged signals; d and e are synchronously averaged high-frequency signals H_6 ($(\omega \geqslant 6\omega_1)$); a) curves *1–13* correspond to $y = 0.35$; 0.70; 1.04; 1.37; 1.78; 2.25; 2.44; 2.63; 3.00; 3.35; 3.80; 4.34; 5.68 mm; $\delta = 4.5$ mm; $\delta_1 = 1.66$ mm; $z = 0$.

are, most likely, responsible for the difference in the spectrum of initial disturbances, namely, the pieces of an adhesive tape under the ribbon in [28] were positioned periodically, while in the present work there was a solitary cut in a thicker piece of the tape. This resulted in the appearance of the periodic pattern of spikes and valleys along z in [28], while a single peak position was observed in the present work.

The stage of development of CS-solitons considered in this section ($x = 450$ mm) corresponds approximately to the coordinate $x = 440$ mm in the K-regime of breakdown studied in [28], as evidenced by the families of both the total oscilloscope traces in Fig. 19c (cf. Fig. 19b) and the high-frequency traces H_6 in

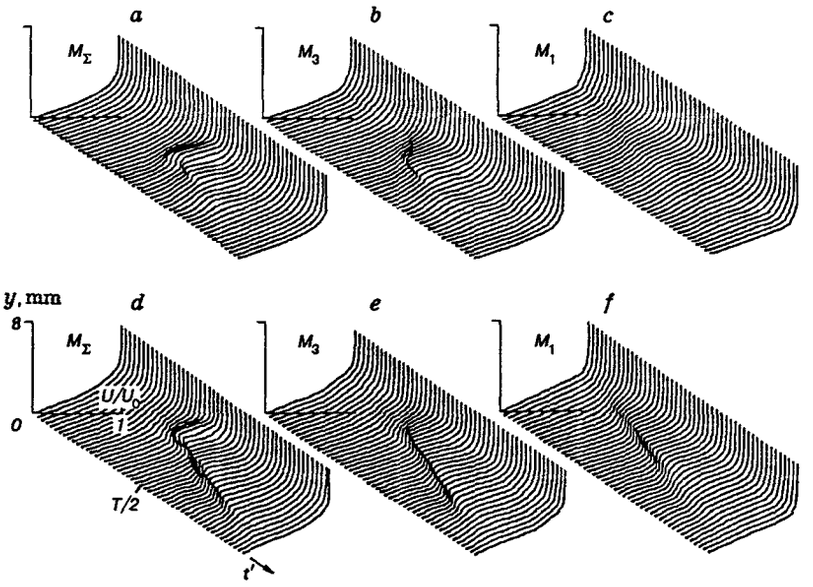

Fig. 20. Instantaneous velocity profiles along y obtained at $x = 450$ mm (a–c) in the present work and at $x = 440$ mm (e, f) in [28]: a, d) are total profiles M_3; b, e) are low-frequency profiles M_3; c, f) are low-frequency profiles M_1; a–c) $t' = t + T/2$; d–f) $t' = t + (29/48)T$; $z = 0$.

Fig. 19e (cf. Fig. 19d). It is in this stage that a rather developed spike which is not yet doubled appears (in the region closer to the wall). The above-mentioned distinctions between the results of observation of this stage and those of [28] are connected mainly with low-frequency disturbances, developing mainly in the near-wall region, and with stationary disturbances of the mean flow.

One of the distinctions of the K-regime with a solitary peak, realized in the present work, is that the high-shear layer is less developed in the stage of appearance of spikes ($x = 450$ mm in the present work and $x = 440$ mm in [28]). This is observed in both mean velocity profiles and instantaneous profiles. The mean velocity profile measured in this work at $x = 450$ mm, where a spike already appears (see Fig. 21a), is very close to the undisturbed one (cf. the profile at $x = 380$ mm from [28] in Fig. 21a) and has no HS-layer or even inflection point. Correspondingly, the region of existence of the instantaneous profiles with the HS-layer in Fig. 20a is also localized more significantly than in the corresponding instantaneous profiles M_Σ from [28], shown in Fig. 20d. Comparison of the low-frequency instantaneous profiles M_3 (Figs. 20b, e) and M_1 (Figs. 20c, f) shows that they are greatly different, as well as the mean velocity profiles (Fig. 21a). In the present case, the low-frequency shear layers are developed very weakly.

With results of the measurements [3, 14], the above comparison indicates that in the version of the K-regime of transition realized in the present work (with a solitary peak along the z-axis), the spikes appear under conditions where the amplitudes of streamwise stationary vortices, which cause the appearance of the HS-layer in the mean velocity profile, are very low (they reach higher amplitudes but at later stages of their development). Similarly, the oscillations of longitudinal vortices at low frequencies have lower amplitudes in this stage. These oscillations form low-frequency instantaneous velocity profiles with the HS-layer, local in time and space, which are very often regarded as the cause of the appearance of flash-spikes through the mechanism of local high-frequency secondary instability (see also [28]).

The above comparison of the properties of disturbances in the stage of appearance of the first soliton shows, in particular, that the role of stationary disturbances (streamwise vortices), arising usually in the K-regime of transition, in the formation of spikes is not as great as is commonly believed. These observations are in good agreement with the conclusion in [28] that the appearance of spike-solitons is not related directly

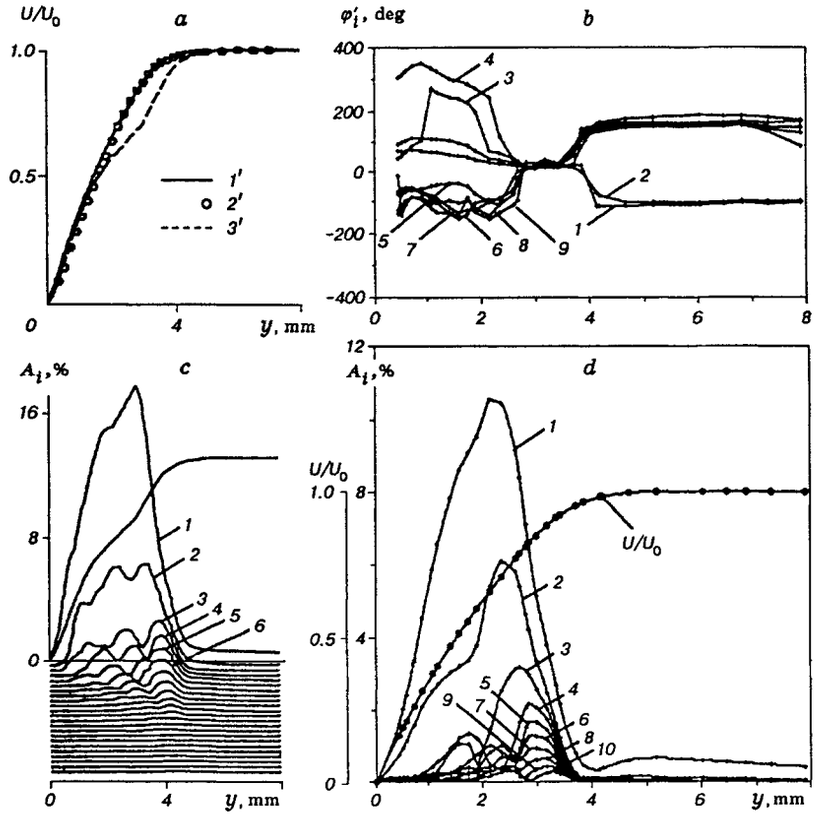

Fig. 21. Profiles of mean velocity (a), amplitudes (c, d), and phases (b) of the frequency harmonics $\omega_1, \ldots, \omega_{10}$ (lines *1–10*), obtained in the present work (b, d, and lines *1'* and *2'* in a) at $x = 450$ mm and in [28] (c and *3'* in a) at $x = 440$ mm; $z = 0$.

to the mechanism of the local high-frequency (inflectional) secondary instability which may develop in the presence of the HS-layers, inasmuch as under the conditions of the present work these layers are very weakly developed in the instantaneous profiles by the moment when the spikes appear and are not present at all in the mean velocity profiles. The low intensity of the HS-layers in the present case has no great impact on the process of generation of CS-solitons. This process proceeds in much the same way as in the presence of strong oscillating streamwise vortices, which usually occur during the periodic spanwise modulation of the primary flow, as observed in [3, 14, 19–21] and elsewhere. As will be shown below, in the present case, the HS-layer develops in the mean velocity profiles (as usual, in the vicinity of the peak position along z) in the later stages of disturbance development, after the first flash-spikes have appeared. It is probably because of the above-indicated circumstances that the initial stages of formation of CS-solitons are very well described by the asymptotic theory [33–36, 41–43] which is purely two-dimensional and does not take into account the existence of streamwise vortices at all.

The stationary three-dimensional disturbances are often given a very significant role in weak-nonlinear approaches used for description of the initial stages of the K-regime of transition (see [12], for example). For instance, the so-called fundamental resonance between the fundamental wave $(\omega_1, 0)$ and the steady modulation of the primary flow $(0, \beta_r)$ is considered one of the causes of generation of three-dimensional modes $(\omega_1, \pm\beta_r)$ ($\pm\beta_r$ are the spanwise wavenumbers). An alternative mechanism was advanced in [22], first studied in [25], and then generalized within the framework of the wave-resonant concept in [7, 8]. It consists in explaining the amplification of the modes of type $(\omega_1, \pm\beta_r)$ by their resonant interaction with the modes

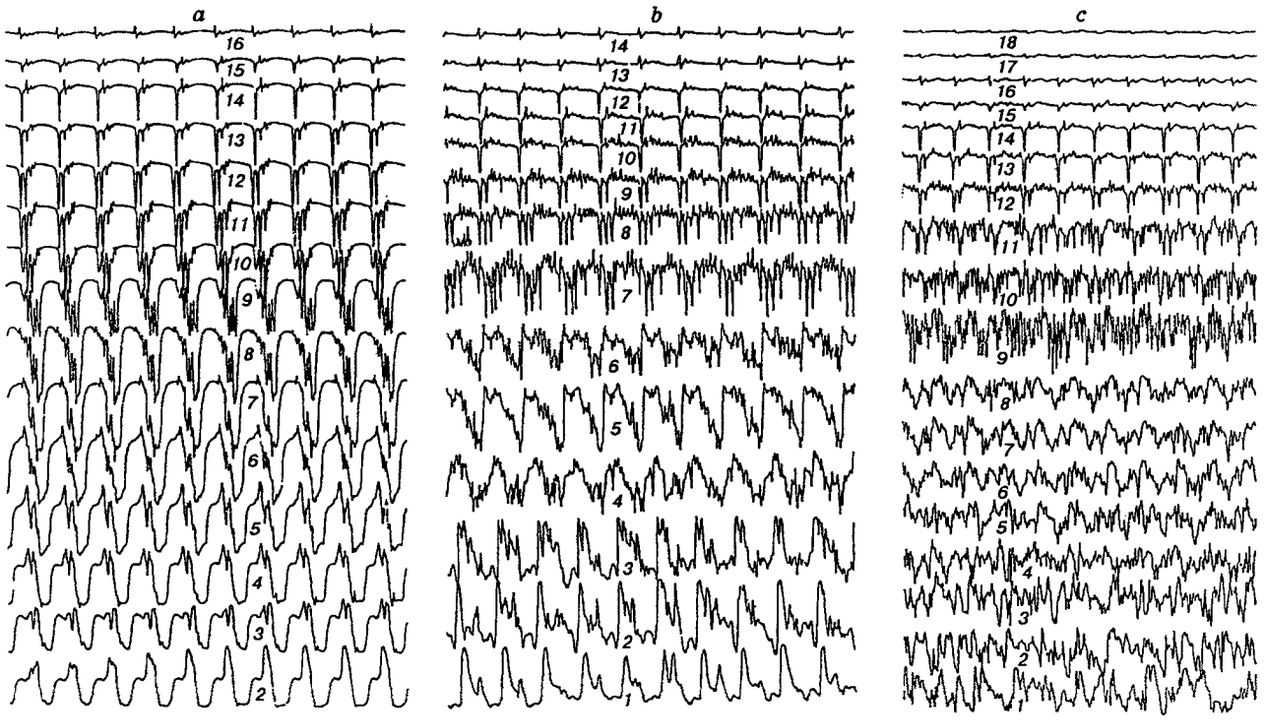

Fig. 22. Dependence of the shape of disturbance oscilloscope traces on y at $z = 0$: a) $x = 500$ mm; curves *2–16* correspond to $y = 0.24$, 0.45, 0.80, 1.09, 1.70, 2.21, 2.76, 3.13, 3.57, 4.15, 4.61, 5.15, 5.67, 6.31, 7.09 mm; $\delta = 6.8$ mm; $\delta_1 = 1.76$ mm; b) $x = 550$ mm; curves *1–14* correspond to $y = 0.18$, 0.51, 0.83, 1.25, 2.09, 3.00, 5.43, 6.00, 6.66, 7.20, 7.84, 8.39, 9.17, 9.95 mm; $\delta = 7.4$ mm; $\delta_1 = 1.53$ mm; c) $x = 600$ mm; curves *1–18* correspond to $y = 0.31$, 0.49, 0.76, 1.43, 1.97, 2.35, 3.31, 3.75, 5.02, 6.05, 6.55, 7.97, 8.85, 9.45, 10.20, 11.00, 12.11, 13.39 mm; $\delta = 8.8$ mm; $\delta_1 = 1.60$ mm.

$(\omega_1, 0)$ and $(2\omega_1, 0)$. It is shown in [44, 45] that the amplification rates of the modes $(\omega_1, \pm\beta_r)$, actually observed in physical [19–21] and numerical [45] experiments, cannot be explained by any of the above types of resonances separately, but in combination they give a good description. However, a very small amplitude of the modes $(0, \beta_r)$ observed in the K-regime of transition, realized in the present work, indicates that the fundamental resonance probably does not play so important a role in the present case.

Let us consider the structure of y-profiles of the amplitudes and phases of various modes in the frequency spectrum. Since the disturbance spectra in the initial stage ($x = 450$ mm) being analyzed consists almost exclusively of the primary wave with frequency ω_1 and its higher harmonics $\omega_n = n\omega_1$, $n = 2, 3, \ldots$ (see Fig. 4), Fig. 21b, d shows the distributions of amplitudes and phases for precisely these harmonics ($n = 1, 2, \ldots, 10$). For comparison, Fig. 21c shows the corresponding amplitude profiles obtained on the basis of data from [28] (for $x = 440$ mm). It is seen that in the present case, as in [28], the amplitude profiles have a form typical for the stage of appearance of the first spike, with an almost clear hierarchy of magnitudes and shapes of the profiles according to the numbers of harmonics.

The maxima of all harmonics, except for the first two or three, are observed in the outer part of the boundary layer below the jump of phases in the phase profiles (at $y/\delta \approx 0.64$–0.73 in Fig. 21d and $y/\sigma \approx 0.80$–0.85 in Fig. 21c). It is in this region that a spike-soliton is observed on the oscilloscope traces and the harmonics' amplitudes attenuate with frequency in an almost strict accordance with the geometric progression (see Figs. 4 and 5). Closer to the wall, the amplitude of each harmonic decreases, though not monotonously but in the form of attenuating beatings, with a gradual shift in position of the beatings' maxima and minima along y as the number n of the harmonic increases (this motion is most clearly seen

in Fig. 21c). Such behavior of the amplitude profiles of higher-frequency harmonics is explained within the framework of the wave-resonant concept [7, 8] by a superposition of eigenfunctions of a set of three-dimensional modes having the same frequency but inclined at different angles to the flow direction and amplified by a system of resonances of subharmonic type.

The most significant distinction of the amplitude profiles in Figs. 21c, d is observed in characteristic scales along y. In the present experiments (Fig. 21d), the profiles are more "pressed" to the wall than in [28] (Fig. 21c). This distinction is, to all appearances, associated with the smaller values of the boundary layer displacement thickness realized in the present work ($\delta = 4.5$ and $\delta_1 = 1.66$ mm), as compared with [28] ($\delta = 4.9$ and $\delta_1 = 2.0$), and this, in turn, results from the lower intensity of streamwise vortices, thickening the boundary layer in the vicinity of the peak. The smaller local thickness of the boundary layer in the present work leads to the zone of spike-soliton's formation approaching the wall, as measured in dimensional coordinates. Moreover, the dimensionless characteristic y-coordinates of the spike position also decrease (see Fig. 21c and d). At the same time, these distinctions do not belittle the above-mentioned general similarity of the amplitude profiles at the stage of appearance of the first developed spike.

The corresponding phase profiles of the fundamental wave and its higher harmonics obtained in the present paper are shown in Fig. 21b. The phases φ_i' correspond to the phase shifts of wave valleys counted off from the time moment that coincides with the cusp of the spike. The profiles clearly show the synchronization of phases of the frequency harmonics in the outer part of the boundary layer, first demonstrated in [19]. The location of the region of phase synchronization ($0.62 \leqslant y/\delta \leqslant 0.76$) coincides with the region of a developed spike on the oscilloscope traces (Fig. 19a, b) and corresponds to the zone of principal maxima in the distributions of higher harmonics' amplitudes along y (Fig. 21d). Closer to the wall, the phases of harmonics are detuned. With distance from the wall the phases of all harmonics undergo a $\pm 180°$ jump typical for the eigenfunctions of both plane and three-dimensional instability waves, and then the phases remain practically constant up to the end of the region of measurements.

Thus, the measurements of the structure of disturbances crosswise the boundary layer conducted at the initial stage of development of CS-solitons showed that this structure is essentially typical for this stage of the K-regime of transition. At the same time, the version of the K-regime realized in the present experiments (with a single peak region along the span, in contrast to periodic peaks in the majority of earlier works) is characterized by a very weak development of the high-shear layer (for the stage of appearance of the first developed spike discussed in this section) in instantaneous velocity profiles (both integral over the spectrum and low-frequency ones) and by the total absence of any high-shear layer (and even an inflection point) in mean velocity profiles.

6.2. *Evolution of the form of oscilloscope traces and instantaneous velocity profiles.* The further development of oscilloscope traces and instantaneous disturbance profiles inside the boundary layer is shown in Figs. 22–26.

Three families of single realizations of velocity oscilloscope traces obtained at different distances from the leading edge are shown in Fig. 22. Similar traces obtained after synchronous averaging are given in Fig. 23.

Typical spikes are seen near the external edge of the boundary layer ($y \approx 5.7$ mm) at $y \approx 500$ mm (Figs. 22a and 23a). Closer to the wall, the number of spikes is doubled, tripled, and so on. This was noticed as early as in the experiments of [2, 3], but for more than 20 years it has been associated with the breakdown of the spikes downstream. The traditional interpretation of the multiplication of spikes as of the process of their breakdown is inadequate to the physical nature of this phenomenon. This misinterpretation is connected with the movement of the forming spike-solitons away from the wall (see Fig. 3 and [28]). The point is that as the probe moves along the x-axis at a constant dimensional distance from the wall, it first falls within a range with the only spike, then with two, three, and so on. This phenomenon was incorrectly considered as the process of breakdown of the spikes downstream.

The true flow pattern is quite different. It is seen from Figs. 22 and 23 that a CS-soliton has a complicated structure along y, which shows itself on the oscilloscope traces in the form of flash-spikes multiplied as they move toward the wall. This structure, as almost all the other properties of the soliton, is practically unchanged and retains all of its main features up to the very late stages of development of the transition

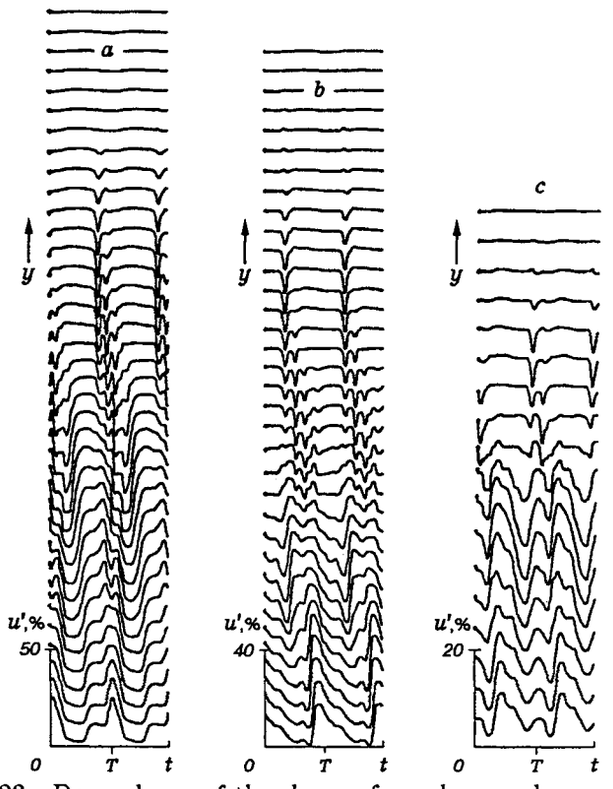

Fig. 23. Dependence of the shape of synchronously averaged oscilloscope traces of disturbances on y at $z = 0$: a–c) $x = 500$, 550, and 600 mm.

process, where the near-wall fluctuations are almost of turbulent character (see curves *1–8* in Fig. 22c). This family of oscilloscope traces with spikes (curves *8–16* in Fig. 22a, *7–14* in Fig. 22b, *9–18* in Fig. 22c, and the corresponding oscilloscope traces in Fig. 23) moves downstream almost as a single whole, i.e., as a coherent structure or an aggregate of coherent structures. The typical time intervals between the 1st and 2nd, 2nd and 3rd, and 3rd and 4th spikes remain practically constant: $\Delta t \approx 1.56$, 1.73, and 1.84 msec, when $x = 500$, 550, and 600 mm, respectively (with a characteristic temporal scale τ of the spike equal to approximately 0.85 msec), or, in dimensionless units of time: $\Delta t^0 = \Delta t U_0/\delta_1 \approx 8.1$, 10.4, and 10.6, when $\tau^0 = \tau U_0/\delta_{1\text{mean}} = 4.8$ ($\delta_{1\text{mean}} = 1.66$ mm, is the mean value of the displacement thickness at $z = 0$).

In the near-wall region of the boundary layer, the structure of disturbances is essentially different. At $x = 500$ mm (Figs. 22a and 23a), in the region where $y \approx 1.2$–2.4 ($y/\delta \approx 0.17$–0.34), the oscilloscope traces begin to take the characteristic shape of a "saw" with teeth formed by a sudden jump in the instantaneous flow velocity from the lower to higher values (with the amplitude reaching 35% of U_0 and 43% of the local mean flow velocity) and by its subsequent smoother decrease accompanied by irregular oscillations (Fig. 22a). These peculiarities of the oscillations in the near-wall region are seen more clearly in the later stages of transition development (Fig. 22b and 23b; $x = 550$ mm). In this stage, the "saw" takes on a more "developed" form and is observed in a wide range of values of the y-coordinate, divided into two subranges (at $y \approx 1.5$–3.8 mm, $y/\delta \approx 0.2$–0.45 and approximately at $y \leqslant 1.5$ mm, $y/\delta \leqslant 0.15$).

It is interesting to note that the "teeth" are observed in the inner part of the boundary layer on the averaged oscilloscope traces up to the very late stages of development. For instance, at $x = 600$ mm, where the fluctuations in single samples (Fig. 22c) taken approximately at $y \leqslant 5$ mm ($y/\delta \leqslant 0.5$) resemble very much the turbulent ones, the averaged oscilloscope traces (Fig. 23c) continue to display the characteristic "teeth" and the saw-like shape of the curves within the range of the y-coordinate, which is as wide as before.

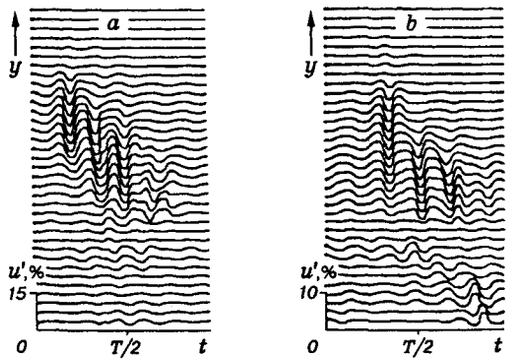

Fig. 24. y-Dependence of the shape of high-frequency synchronously averaged oscilloscope traces H_6 at $z = 0$: a,b correspond to $x = 500$, 550 mm.

Figure 24 presents families of oscilloscope traces of high-frequency disturbances (within the frequency range H_6, i.e., starting with the frequency $6\omega_1$ and higher) obtained from the averaged oscilloscope traces shown in Figs. 23a, b. It is obvious that in the stage of a developed CS-soliton, almost the whole energy of the deterministic high-frequency disturbances that are coherent with the fundamental wave is concentrated in the soliton. One can easily see the high-frequency components of the 1st, 2nd, 3rd, and even 4th spike, which are located in the outer part of the boundary layer (at $y \approx 2.6$–6.4 mm and $y/\delta \approx 0.37$–0.9 mm, when $x = 500$ mm, and at $y \approx 4.4$–8.8 mm and $y/\delta \approx 0.55$–1.10, when $x = 550$ mm) and move downstream, almost without changing their form and mutual arrangement.

Thus, the oscilloscope traces, obtained in different stages development of disturbances at different distances from the wall, clearly show a separation of the disturbances into fluctuations of two kinds. The first of these includes disturbances associated with CS-solitons which are observed in an extensive outer part of the boundary layer (at $y/\delta \gtrsim 0.5$) and have the typical shape of spikes. The second are near-wall fluctuations which appear on the oscilloscope traces in the form of a "saw" with characteristic velocity jumps (teeth) and are also observed over a wide range of values of the y-coordinate (at $y/\delta \lesssim 0.5$). This separation occurs in the early stages of development of CS-solitons and is preserved until the very late stages ($x = 600$ mm), when the flow in the near-wall region becomes highly turbulent.

It is interesting to compare the properties of these two types of disturbances both with each other and with the properties of instantaneous velocity profiles observed in the stages of developed CS-solitons and shown in Figs. 25 and 26. These results (as many others in this work) supplement the analogous data of [28] obtained in the region of the late stages of development of CS-solitons.

The instantaneous profiles shown in Figs. 25 and 26 were obtained by one-point measurements (by making a section of the arrays of the disturbance oscilloscope traces in Fig. 23 along $t = \text{const}$ in combination with their frequency filtration). Therefore, they reflect only the evolution of the periodic (with fundamental period $T = 1/f_1$) component of fluctuations, which dominates only in the initial stage. Afterwards, the increasingly substantial aperiodic (stochastic) component appears, which, in measurements of the instantaneous profiles, manifests itself as a noise increasing downstream.

Three families of instantaneous total velocity profiles M_Σ and low-frequency profiles M_3 and M_1 are shown in Fig. 25a–c for $x = 500$ mm. The local velocity defects are easily seen in the total profiles (Fig. 25a). They are attributed to the 1st, 2nd, and, partially, the 3rd spike on oscilloscope traces (in the vicinity of profiles *14-16*, *21-23*, and *28–30*, respectively). In the temporal region that approximately corresponds to the third spike (from the *26*th profile and later on) an HS-layer appears and moves gradually toward the wall. It should be noted at once that the delay in time between the phases of existence of spikes (associated with CS-solitons) and those of the HS-layer, within the fundamental period, changes constantly during the

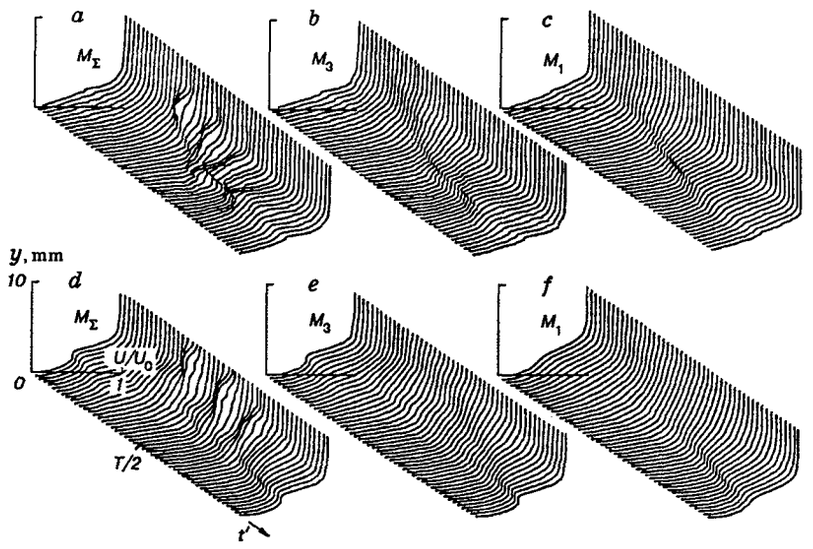

Fig. 25. Instantaneous velocity profiles along y obtained at $x = 500$ mm (a–c) in the present work and at $x = 490$ mm (d–f) obtained in [19–21]: a, d) profiles M_Σ integrated over spectrum; b, e) low-frequency profiles M_3; c, f) low-frequency profiles M_1; a–c) $t' = t + T/2$; d–f) $t' = t$; $z = 0$.

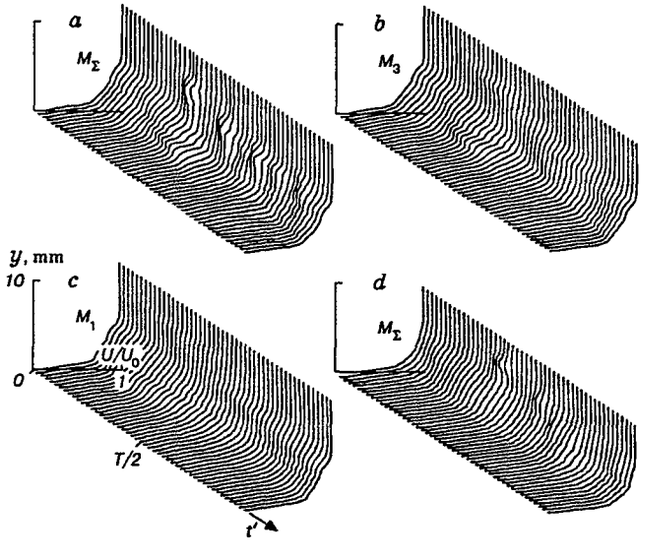

Fig. 26. Instantaneous velocity profiles along y, obtained at $x = 550$ mm (a–c) and at $x = 600$ mm; a, d) total profiles M_Σ; b) low-frequency profiles M_3; c) low-frequency profiles M_1; a–c) $t' = t$; d–f) $t' = t + T/2$; $z = 0$.

displacement along x and cannot be regarded as a characteristic of the disturbance development. In particular, this is clearly seen when comparing the instantaneous profiles M_Σ shown in Fig. 25a ($x = 500$ mm) and in Fig. 26a ($x = 550$ mm). In the latter figure, the HS-layer is observed in the vicinity of the first spike, not of the third one, as in the case of $x = 500$ mm.

Also a comparison of instantaneous velocity profiles M_Σ in Fig. 25a ($x = 500$ mm) with analogous profiles in Fig. 25d, which were obtained by processing the results of experiments in [19–21] (as well as in Fig. 25e, f) points to the absence of the phase relation between the CS-soliton and CS-layer. The coordinate $x = 490$ mm in [19–21] corresponds approximately to the coordinate $x = 500$ mm in the present work. However,

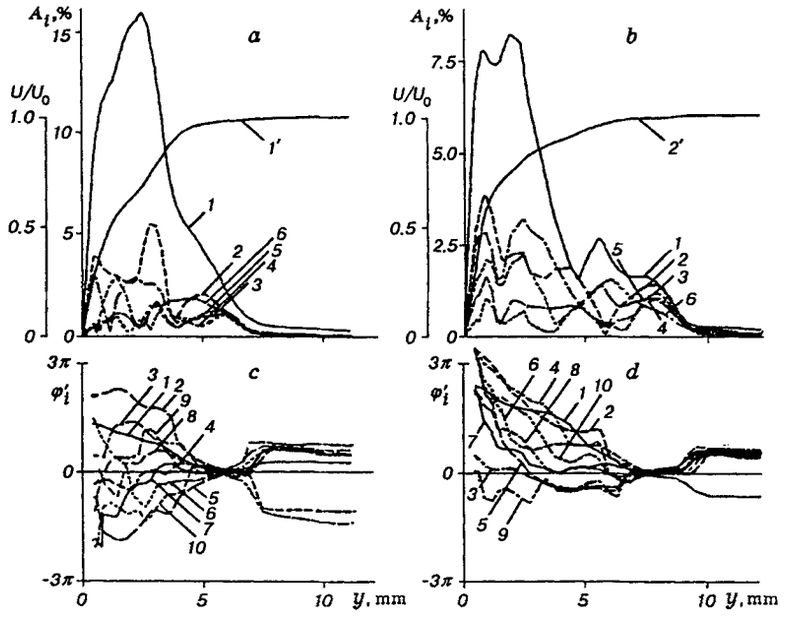

Fig. 27. Distributions of amplitudes (a, b) and phases (c, d) of frequency harmonics along y at $x = 500$ (a, c) and 550 mm (b, d), and the corresponding mean velocity profiles (*1′* and *2′*): curves *1–10* correspond to $\omega_1, \ldots, \omega_{10}$; $z = 0$.

as one can see, the HS-layer in Fig. 25d has an essentially different phase at the period of the fundamental wave, as compared to the place of the CS-soliton (in this case, they are approximately in antiphase).

The low-frequency instantaneous profiles M_1 and M_3 shown in Fig. 25b, c (as well as the profiles in Fig. 25e, f, obtained from the processing of data in [19–21]) clearly show an HS-layer and illustrate its low-frequency nature. At the same time, the high-frequency disturbances corresponding to the CS-soliton (i.e., to the spikes) are not observed in the profiles M_1 and M_3.

At $x = 500$ mm, the CS-soliton structure is also clearly seen in the instantaneous profiles M_Σ (Fig. 26a) in the form of sequential local linear falls. Apart from the first three spikes (profiles *16–18*, *24–26*, and *32–34*), the fourth spike is also seen in this case (profiles *41–43*). The HS-layer is clearly seen in this stage in the instantaneous profiles M_Σ and M_3 (Fig. 26a, b, in the region below the first spike) and is much less developed than at $x = 500$ mm (Fig. 25a, b). The interval of its existence in time (and, consequently, in space along the streamwise coordinate, too) is also significantly (several times) less than at $x = 500$ mm. Furthermore, at $x = 500$ mm the HS-layer looks approximately the same in the instantaneous profiles M_Σ and M_3, and in the profile M_1 it is already not noticeable at all (Fig. 26c). This means that the fundamental wave (with frequency ω_1) makes no essential contribution to its formation.

At $x = 600$ mm, the first and second spikes (profiles *18–20* and *26–28*) continue to be clearly seen in the profiles M_Σ (Fig. 26d). However, the HS-layer is practically unobservable in this stage. Naturally, it is absent in the low-frequency profiles M_3 and M_1, which are very filled in this region all the time and begin to resemble the profiles of turbulent flow.

The absence of the third and fourth spikes in the CS-soliton structure at $x = 600$ mm in Fig. 26d (and also in Fig. 23c) is, most likely, associated with their strong unsteadiness, which is seen in Fig. 22c. The amplitude and phase of the spikes in this region strongly vary under the action of turbulent fluctuations, amplified inside the boundary layer. The degree of nonperiodicity of the spikes (i.e., the magnitude of their amplitude and phase "joltiness") increases not only downstream but also during displacement toward the

wall. Since the characteristic y-coordinate of the spike increases with an increase in its ordinal number (see Figs. 22–24) and spikes with large ordinal numbers are located closer to the highly turbulent near-wall region, the unsteadiness of each subsequent spike increases too. At $x = 600$ mm, the procedure of synchronous averaging (when the signal fed to the ribbon is used as the reference one) leads to the negative interference of the third and fourth spikes because of their high phase unsteadiness. For this reason, these spikes are not seen both on the averaged oscilloscope traces and in the instantaneous profiles as early as at $x = 600$ mm (although they are seen in the isolated realizations in Fig. 22c).

6.3. *Evolution of y-distributions of spectral characteristics.* The subsequent downstream development of the normal-to-wall distributions of amplitudes and phases of the frequency harmonics (shown in Fig. 21c, d for $x = 450$ mm) is illustrated in Fig. 27a, b for modes with frequency ω_1 and its higher harmonics $\omega_2, \ldots, \omega_5$ at $x = 500$ and 550 mm, respectively (the mean flow velocity profiles are also shown there). A comparison of the amplitude profiles with those presented in Fig. 21d ($x = 450$ mm) shows that their main peculiarity — the presence of a local maximum in the y-coordinate region where the spikes on the oscilloscope traces are present (i.e., in the region of the CS-soliton) — remains unchanged in the later stages of the disturbance development: at $y \approx 2.6$–6.4 mm ($y/\delta \approx 0.37$–0.9), when $x = 500$ mm, and at $y \approx 4.4$–8.8 mm ($y/\delta \approx 0.55$–1.10), when $x = 550$ mm. In the near-wall region, however, the disturbance intensity grows significantly, as compared with $x = 450$ mm, and a randomization of the flow occurs there.

The profiles of disturbance phases, in the stages of development presented in Fig. 27, remain very similar to those observed in the stage of CS-solitons' formation (Fig. 21b). In the outer part of the boundary layer (and outside it), the phases remain synchronized. Moreover, the accuracy of their synchronization does not decrease downstream and the number of harmonics having a high degree of synchronization even increases at $x = 550$, as compared with $x = 450$ and 500 mm. An important feature of the profiles of the amplitudes and phases of the frequency harmonics constituting the spikes consists in the conservation of their properties in the outer part of the boundary layer and — surprising as it may seem — their local similarity with the properties of the eigenfunctions of instability modes. In particular, the phase profiles of all the frequency harmonics still demonstrate the constancy of the phase outside the boundary layer, the phase jump by approximately π in the region of its external edge, and then, again, the constancy of the phase in the region below the jump. As in the profiles of eigenfunctions of three-dimensional instability modes (see [51, 52], for example), the amplitudes of the frequency harmonics are very low in the region above the phase jump, and begin to rapidly grow when displacing toward the wall immediately after the phase jump. At the same time, closer to the wall the behavior of the phases of higher harmonics of the fundamental wave differs essentially from the linear one, although it remains very regular up to $x = 550$ mm (Fig. 27b and d). In the near-wall region, a three-dimensional HS-layer develops and turbulence begins to arise.

In even later stages ($x = 570$ and 590 mm), thoroughly studied within the framework of experiments of [19, 20] (these data have not been published so far) and presented in Fig. 28, the mean velocity profiles *11* and the total disturbance intensity *7* become absolutely typical for the developed turbulent regime.

At the same time, even in these stages the local peak in the distributions of the frequency harmonics' amplitudes, observed in the region of existence of the coherent structure–spikes (at $y \approx 6$ and 8 mm in Fig. 27a, b, respectively), is still clearly seen far from the wall. It is this peak that produces a rise in the profile of total fluctuations (at $y \approx 8$ mm; Fig. 28a, b), which is so typical for a developed turbulent flow and is observed in numerous measurements, starting with the classical experiments by Klebanoff (see reference [20] in Chapter XVIII of [53]). The well-known similarity of the K-regime of transition in a boundary layer and in a flat-channel flow [32] is probably responsible for the fact that the above-mentioned rise in the profile of total fluctuations is also observed in channels, starting with experiments by Reihardt (see reference [32] in Chapter XVIII of [53]). First, these results may be regarded as additional evidence for the correctness of the notion of the developed near-wall turbulent flow as a continuous K-regime of transition to turbulence (as suggested in [9, 39, 40]). Second, they point to the close relation between CS-solitons and the shape of the profile of turbulent fluctuations far from the wall.

6.4. *Vortex structure of the disturbance field.* As was shown in Sec. 6.2, the separation of deterministic (i.e., coherent with the fundamental wave) disturbances into two types (termed by convention in [28] the

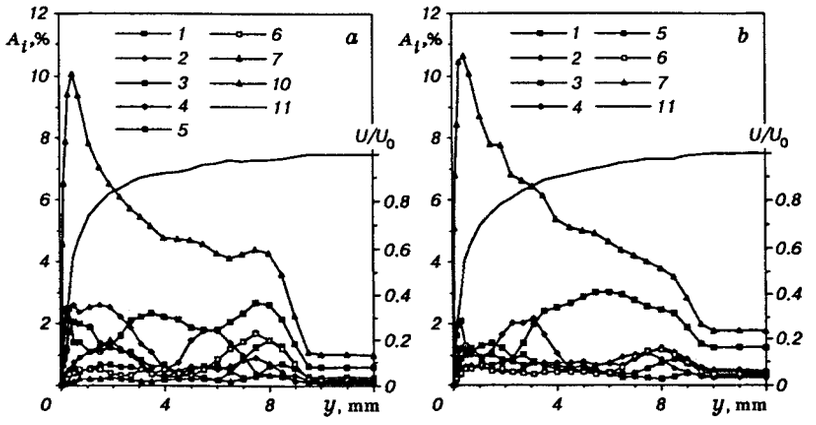

Fig. 28. Distributions of amplitudes of frequency harmonics along y according to the experimental data in [19, 20] at $x = 570$ and 590 mm (a and b): curves *1–6* and *10* correspond to $\omega_1, \ldots, \omega_6$, and ω_{10}; *7*) amplitudes of total fluctuations; *11*) mean velocity profiles; $z = 0$.

upper and lower ones) is preserved far downstream. The upper structures are associated with CS-solitons (spikes) and the lower ones are associated with the high-shear layer (see Figs. 25 and 26). The jumps in the streamwise flow-velocity component, termed the "teeth"and observed on the oscilloscope traces in the near-wall region (Figs. 22b, 23b, c), also represent long-lived coherent disturbances which are, probably, connected with the high-shear layer (HS-layer). The task of this section is to check whether or not there is a relation among the coherent disturbances, and between these and the vortex structure of the flow in the vicinity of the peak ($z = 0$).

The instantaneous profiles of flow-velocity disturbance, described in Secs. 6.1 and 6.2, were used to study the instantaneous vortex structure of the flow. To diminish the measurement error that inevitably occurs with differentiation of experimental data, the profiles were smoothed by means of their approximation by cubic splines. After that, the fields of the $\partial\hat{u}/\partial y$ values were determined ($\hat{u}$ is the disturbance of the streamwise flow-velocity component coherent with the fundamental wave).

The downstream evolution of the instantaneous field of the $\partial\hat{u}/\partial y$ values measured in the plane (y,t) is shown in Figs. 29 and 30 in the form of contours. In the boundary layer these values are very close to the corresponding fields of the lateral component ω_z' of the instantaneous vorticity vector of the flow disturbances. Note that the (y,t) plane is equivalent effectively to the $(y,-x)$ plane, provided that the structures are frozen locally. The high "ridges" (by analogy with a geographic map) with a large positive value of vorticity correspond to the HS-layer, which is formed in the near-wall region and stretched moving downstream. Points *5* in Figs. 29 and 30 display the location of the "teeth" (see Fig. 23) in the (y,t)-plane at the moment of intersection of the trace with the zero level. As is seen, these points coincide with the HS-layer for all values of the coordinates y and t (in the stages of development where the "teeth" and HS-layer are observed). This means that the high-shear layer in the instantaneous profiles (see Figs. 25 and 26) and the "teeth" on the oscilloscope traces (see Fig. 23) represent two different manifestations of the same vortex formation — near-wall coherent structure.

It is seen from Fig. 29 that some vortex structures in the form of pairs of counter-rotating vortices separate from the forming HS-layer and start to propagate in the outer part of the boundary layer [the first of these structures separates in the very early stages of development ($x \approx 450$ mm), where the HS-layer is still rather weakly developed]. The black dots in Figs. 29 and 30 show the regions in the (y,t) plane where spikes can be identified on the oscilloscope traces (see Figs. 19b and 23). The spikes reach their maximum amplitudes at points marked with crosses. In all stages of the disturbance development the location of the spikes is seen to coincide with the location of these pairs of counter-rotating vortices. The maximum amplitudes of the spikes

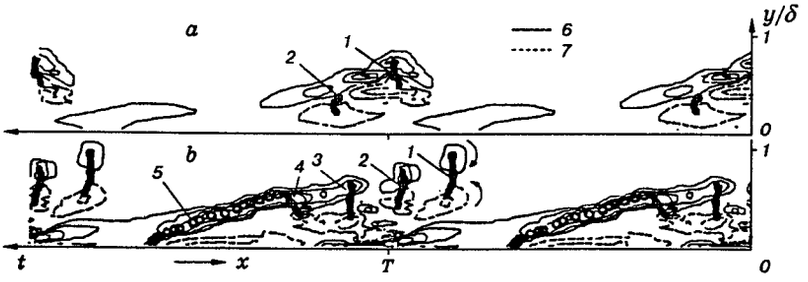

Fig. 29. Qualitative structure of the field of instantaneous spanwise vorticity of the flow: contours of $\partial\hat{u}/\partial y$ at $x = 450$ and 500 mm (a, b); solid lines for $\partial\hat{u}/\partial y > 0$ and dashed lines for $\partial\hat{u}/\partial y < 0$; points *1–4* designate the places where the 1st, 2nd, 3rd, and 4th spikes can be identified on the oscilloscope traces; the points marked with crosses designate the position where the spike has a maximum amplitude; *5* is the location of "teeth" on the oscilloscope traces at the point of intersection with the level of the mean velocity value; $z = 0$.

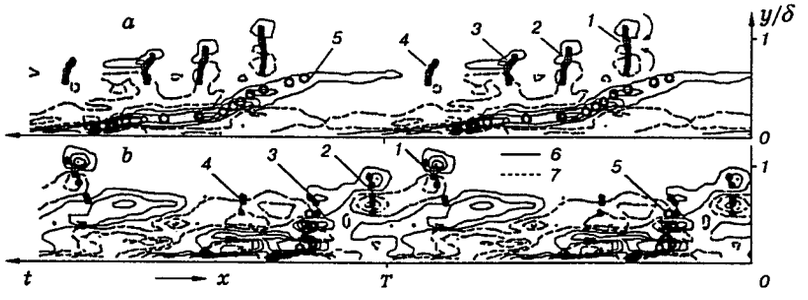

Fig. 30. See Fig. 29 for caption [$x = 550$ and 600 mm (a, b)].

are observed in a gap between the vortices. The vortices "float up" together with the spikes in the direction of the external edge of the boundary layer and accelerate up to a speed close to that of the potential flow. This means that the CS-solitons discussed above and the vortex pairs in Figs. 29 and 30 are the same objects, namely, the soliton-like coherent structures (associated with the spikes on oscilloscope traces).

It is natural to assume that the vortex pairs in Figs. 29 and 30 represent the sections of ring-like (toroidal) vortices by the plane $z = 0$, with the vortex axis oriented upstream. It is the intensive rotation of such a ring-like "pretzel" that leads to an abrupt fall (for a short period of time) of the streamwise velocity component, registered as a spike on the oscilloscope trace when the ring-like vortex flies past the point where the hot-wire probe is located. Four such vortices manage to form at each period of the fundamental wave. They have their own spatial (and temporal) scale, which is not related to the length (and period) of the primary instability wave. As early as in the vicinity of $x = 550$ mm, these vortex structures, moving at a high speed (see Fig. 8), catch up with the HS-layer that has formed at the previous period of the fundamental wave (Fig. 30a).

Note that the configuration of the field of instantaneous vorticity of the flow in the initial stage of development of the HS-layer (Fig. 29a) is in good qualitative agreement with the data in [14] and with results of direct numerical simulation of the K-regime of transition [45, 47]. Formation of the ring-like vortices in the late stages of transition in the front part of the Λ-like structures was noted as early as in experiments [17, 54], and also in numerical experiments [45, 46], and in others. A series (of 3 or 4 vortices) of ring-like vortices is formed at each period of the fundamental wave in numerical simulation on the basis of the Navier–Stokes equations [45, 46], as in the present experiments. The results of the present experiments and [14, 17, 45–

47, 54] allow the conclusion that, in the late (essentially three-dimensional) stages of their development, the CS-solitons, registered as spikes on oscilloscope traces, are ring-like vortex structures, observed in a series of visualization experiments and in numerical experiments. These structures, as mentioned in [10, 13, 39, 40], are in close relation with coherent structures ("typical vortices" [55]) observed in the outer part of the developed turbulent boundary layer. Therefore, the investigation of them is of great interest for understanding the physical nature of near-wall turbulence as a continuous K-regime of transition with sporadic formation of coherent structures (including those of CS-soliton type) [13].

Thus, a detailed experimental study of the development of coherent structures in the late stages of the K-regime of the boundary-layer transition to turbulence has been conducted in this work. The data obtained allow one to draw the following conclusions.

1. The separation of coherent disturbances, occurring in comparatively early stages of transition (and noted in [28]), into two groups — the near-wall ones, associated with the high-shear layer, and the soliton-like coherent structures (CS-solitons) — is conserved up to the very late stages of development, up to the almost developed turbulent regime.

2. At each period of the fundamental wave several coherent structures, associated with spikes on the velocity oscilloscope traces, are formed. In the early stages of development, these structures are very well described by soliton solutions within the framework of the asymptotic theory [43], and in the late stages they concentrate into very localized toroidal vortex formations with characteristic scales of the order of the boundary-layer thickness. They propagate in the outer part of the boundary layer at velocities close to the potential flow velocity. The properties of these coherent structures are quite conservative and remain practically unchanged from the moment when their formation has been completed up to the almost full transition of the flow to the turbulent state.

3. The high-shear layer in the instantaneous velocity profiles, which is formed in the near-wall region, propagates half as quickly as the soliton-like structures. It stretches along the streamwise coordinate and breaks down (while the CS-solitons continue to propagate downstream, as if not noticing the transition of the flow to turbulence occurring inside the boundary layer, though they probably take part in that transition).

4. The experimental results obtained are in good agreement with those of the previous experiments (e.g., [14, 17, 54]) and with direct numerical simulations of the transition process (e.g., [45–47]), and make it possible to clarify considerably the flow structure and the properties of the coherent disturbances in the late stages of the K-regime of transition.

5. However, a number of important questions still remained to be answered and require further investigation. First of all, there is the question of the specific role that each type of the above coherent structures plays in the process of the final breakdown and randomization of the laminar flow. It is also unclear whether these structures interact with each other in the late stages of development or develop independently. At the same time, it seems obvious that it is these two types of coherent disturbances that form the principal structure of the flow in the late stages of transition and cause laminar-turbulent transition of the flow.

REFERENCES

1. G. B. Schubauer and H. K. Skramstad, "Laminar boundary-layer oscillations and transition on a flat plate," *J. Res. Natl. Bur. Stand.*, **38**, 251–292 (1947).
2. P. S. Klebanoff and K. D. Tidstrom, "Evolution of amplified waves leading to transition in a boundary layer with zero pressure gradient," Tech. Note / NASA; D-195, Washington (1959).
3. P. S. Klebanoff, K. D. Tidstrom, and L. M. Sargent, "The three-dimensional nature of boundary layer instability," *J. Fluid Mech.*, **12**, 1–34 (1962).
4. Y. S. Kachanov, V. V. Kozlov, and V. Y. Levchenko, "Nonlinear development of a wave in a boundary layer," *Izv. Akad. Nauk SSSR, Mekh. Zhidk. Gaza*, No. 3, 49–58 (1977). [Translation in Fluid Dynamics, **13**, 704–711 (1979).]

5. Y. S. Kachanov and V. Y. Levchenko, "Resonant interaction of disturbances upon transition to turbulence in a boundary layer," Preprint No. 10-82, Inst. Theor. and Appl. Mech., Siberian Div. USSR Acad. Sci. [in Russian], Novosibirsk (1982).
6. Y. S. Kachanov and V. Y. Levchenko, "The resonant interaction of disturbances at laminar-turbulent transition in a boundary layer," *J. Fluid Mech.*, **138**, 209–247 (1984).
7. Y. S. Kachanov, "Resonant-wave nature of transition to turbulence in a boundary layer," in: *Modeling in Mechanics* [in Russian], Proc. Siberian Div., Ist Theor. and Applied Mechanics, **1**(18), No. 2, 75–98 (1987).
8. Y. S. Kachanov, "On the resonant nature of the breakdown of a laminar boundary layer," *J. Fluid Mech.*, **184**, 43–74 (1987).
9. Y. S. Kachanov, "Resonant-wave nature of breakdown of a boundary layer," in: *Models of Mechanics of Continuous Medium* [in Russian], Vladivostok (1989), pp. 66–93.
10. Y. S. Kachanov, "Resonant-soliton nature of boundary layer transition," *Russian J. Theor. Appl. Mech.*, **1**, No. 2, 141–173 (1991).
11. T. Herbert, "Secondary instability of boundary layers," *Annu. Rev. Fluid Mech.*, **20**, 487–526 (1988).
12. A. H. Nayfeh, "Nonlinear stability of boundary layers," AIAA paper, No. 87-0044, New York (1987).
13. Y. S. Kachanov, "Physical mechanisms of laminar-boundary layer transition," *Annu. Rev. Fluid Mech.*, **26**, 411–482 (1993).
14. L. S. Kovasznay, H. Komoda, and B. R. Vasudeva, "Detailed flow field in transition," Heat Transfer and Fluid Mech. Inst.: Proc. Annu. Meeting, Washington, Stanford (1962), pp. 1–26.
15. J. Tani and H. Komoda, "Non-linear development of disturbances in the laminar boundary layer," *J. Aerosp. Sci.*, **29**, No. 4, 440 (1962).
16. H. Komoda, "Non-linear development of disturbances in the laminar boundary layer," *Phys. Fluids Suppl.*, **10**, S87–S94 (1967).
17. F. R. Hama and J. Nutant, "Detailed flow-field observations in the transition process in a thick boundary layer," Heat Transfer and Fluid Mech. Inst.: Proc. Annu. Meeting, Pasadena, 1963. Stanford, (1963), pp. 77–93.
18. Y. S. Kachanov, V. V. Kozlov, and V. Y. Levchenko, *Occurrence of Turbulence in Boundary Layers* [in Russian], Naūka, Novosibirsk (1982).
19. Y. S. Kachanov, V. V. Kozlov, V. Y. Levchenko, and M. P. Ramazanov, "Experimental study of the K-regime breakdown of a laminar boundary layer," Preprint No. 9-84, Inst. Theor. and Appl. Mech., Siberian Div. USSR Acad. Sci., Novosibirsk (1984).
20. Y. S. Kachanov, V. V. Kozlov, V. Y. Levchenko, and M. P. Ramazanov, "On the nature of K-breakdown of a laminar boundary layer," in: *Laminar Turbulent Transition*, Springer, Berlin (1985), pp. 61–73.
21. Y. S. Kachanov, V. V. Kozlov, V. Y. Levchenko, and M. P. Ramazanov, "The nature of the K-regime of breakdown of a laminar boundary layer," *Izv. Sib. Otd. Akad. Nauk SSSR, Ser. Tekh. Nauk*, No. 2, 124–158 (1989).
22. A. D. D. Craik, "Nonlinear resonant instability in boundary layers," *J. Fluid Mech.*, **50**, 393–413 (1971).
23. M. B. Zelman and I. I. Maslennikova, "Resonant amplification of spatial disturbances in boundary layers," in: *Instability of Sub- and Supersonic Flows* [in Russian], Inst. Theor. and Appl. Mech., Siberian Div. USSR Acad. Sci., (1982), pp. 5–15.
24. T. Herbert, "Analysis of the subharmonic route to transition in boundary layers," AIAA paper No. 84-0009, New York (1984).
25. A. H. Nayfeh and A. N. Bozatli, "Nonlinear wave interactions in boundary layers," AIAA paper No. 79-1456, New York (1979).
26. V. I. Borodulin, S. V. Dryganets, Y. S. Kachanov et al., "Receptivity of a transitional boundary layer to small background disturbances," in: *Problems of Modeling in Wind Tunnels* [in Russian] Int. Seminar, July 25–29, 1988, Novosibirsk, Vol. 1 (1989), pp. 107–116.

27. V. I. Borodulin and Y. S. Kachanov, "Cascade of harmonic and parametric resonances in the K-regime of boundary layer breakdown," in: *Modeling in Mechanics* [in Russian], Inst. Theor. and Appl. Mech., Siberian Div. USSR Acad. Sci., **3(20)**, No. 2, 38–45 (1989).
28. V. I. Borodulin and Y. S. Kachanov, "Role of the mechanism of local secondary instability in the K-breakdown of a boundary layer," *Izv. Sib. Otd. Akad. Nauk SSSR, Ser. Tekh. Nauk*, No. 5, 65–77 (1988).
29. R. Betchov, "On the mechanism of turbulent transition," *Phys. Fluids*, **3**, 1026–1027 (1960).
30. H. F. Greenspan and D. J. Benney, "On shear-layer instability, breakdown and transition," *J. Fluid Mech.*, **15**, 133–153 (1963).
31. M. T. Landahl, "Wave mechanics of breakdown," *J. Fluid Mech.*, **56**, No. 4, 755–802 (1972).
32. M. Nishioka, M. Asai, and S. Isida, "An experimental investigation of the secondary instability," in: *Laminar-Turbulent Transition*, Springer, Berlin (1980), pp. 37–46.
33. V. I. Zhuk and O. S. Ryzhov, "On locally inviscid disturbances in boundary layers with self-induced pressure," *Dokl. Akad. Nauk SSSR*, **263**, No. 1, 56–59 (1982).
34. F. T. Smith and O. R. Buggraf, "On the development of large-sized short-scaled disturbances in boundary layers," *Proc. Roy. Soc. London. Ser. A.*, **399**, No. 1816, 25–55 (1985).
35. A. P. Rothmayer and F. T. Smith, "Strongly nonlinear wave-packets in boundary layers," *Trans. ASME*, Ohio, Cincinnati, 67 (June 1987).
36. O. S. Ryzhov and I. V. Savenkov, "Asymptotic approach to hydrodynamic stability theory," *Mat. Modelirovanie*, **1**, No. 4, 61–68, (1989).
37. V. I. Borodulin and Y. S. Kachanov, "Coherent structure-solitons in a boundary layer and mechanism of their formation," in: Modern Problems in Fluid and Gas Mechanics [in Russian] , Irkutsk (1990), pp. 65–66.
38. V. I. Borodulin and Y. S. Kachanov, "Experimental study of soliton-like coherent structures in boundary layer," Proc. 19th Session, Scientific and Methodological Seminar on Ship Hydrodynamics, Varna, Bulgaria, Vol. 2 (1990), pp. 99-1–99-10.
39. Y. S. Kachanov, "Secondary and cascade resonant instabilities of boundary layers. Wave-resonant concept of a breakdown and its substantiation," in: *Laminar-Turbulent Transition*, Springer, Berlin (1990), pp. 65–80.
40. Y. S. Kachanov, "The mechanisms of formation and breakdown of soliton-like coherent structures in boundary layers," in: *Advances in Turbulence* Vol. 3, Springer, Berlin (1991), pp. 42-51.
41. O. S. Ryzhov, "On the formation of ordered vortex structures from unstable oscillations in a boundary layer," *Zh. Vychisl. Mat. Mat. Fiz.*, **29**, No. 12, 1804–1814 (1990).
42. Y. S. Kachanov and O. S. Ryzhov, "Formation of solitons in transitional boundary layer: theory and experiment," *Sib. Fiz.-Tekh. Zh.*, No. 1, 34–52 (1992).
43. Y. S. Kachanov, O. S. Ryzhov, and F. T. Smith, "Formation of solitons in transitional boundary layers: theory and experiment," *J. Fluid Mech.*, **251**, 273–297 (1993).
44. H. Fasel, "Numerical simulation of instability and transition in boundary layer flows," in: *Laminar-Turbulent Transition*, Springer, Berlin (1990), pp. 587–598.
45. U. Rist, "Numerische Untersuchung der räumlichhen, dreidimensionalen Störungsentwicklung beim nzschichtumschlag," Diss., Institute A für Mechanik der Universität Stuttgart, Stuttgart (1990).
46. U. Rist and H. Fasel, "Spatial three-dimensional numerical simulation of laminar-turbulent transition in a flat-plate boundary layer," Boundary Layer Transition and Control Conference, Cambridge, U.K. (1991), pp. 25.1–25.9.
47. L. Kleiser and T. A. Zang, "Numerical simulation of transition in wall-bounded shear-flows," *Annu. Rev. Fluid Mech.*, **23**, 495–537 (1991).
48. S. V. Dryganets, Y. S. Kachanov, V. Y. Levchenko, and M. P. Ramazanov, "Resonant flow randomization in the K-regime of boundary layer transition," *Prikl. Mekh. Tekh. Fiz.*, No. 2, 83–94 (1990).

49. Y. S. Kachanov, V. V. Kozlov, and V. Y. Levchenko, "The development of small-amplitude oscillations in a laminar boundary layer," *Uch. Zap. TsAGI.*, **6**, No. 5, 137–140 (1975).
50. Y. S. Kachanov and A. Michalke, "Three-dimensional instability of flat-plate boundary layers: Theory and experiment," *Eur. J. Mech. B/Fluids*, **13**, No. 4, 401–422 (1994).
51. V. M. Gilyov, Y. S. Kachanov, and V. V. Kozlov, "Development of a spatial wave packet in a boundary layer," Preprint No. 34-81, Inst. Theor. and Appl. Mech., Siberian Div. USSR Acad. Sci., Novosibirsk (1981).
52. V. M. Gilyov, Y. S. Kachanov, and V. V. Kozlov, "Development of a spatial wave packet in a boundary layer," *Izv. Sib. Otd. Akad. Nauk SSSR, Ser. Tekh. Nauk*, No. 13, No. 3, 27–37 (1983).
53. G. Schlichting, *Theory of Boundary Layers* [in Russian], Nauka, Moscow (1969).
54. C. F. Knapp and P. J. Roache, "A combined visual and hot-wire anemometer investigation of boundary-layer transition," *AIAA J.*, **6**, No. 1, 29–36 (1968).
55. R. E. Falco, "Coherent motions in the outer region of turbulent boundary layers," *Phys. Fluids Suppl.*, **20**, No. 10, S124–S132 (1977).